# ROBUST LEVEL-SET-BASED TOPOLOGY OPTIMIZATION UNDER UNCERTAINTIES USING ANCHORED ANOVA PETROV-GALERKIN METHOD

CHRISTOPHE AUDOUZE[*], AARON KLEIN[*], ADRIAN BUTSCHER[†], NIGEL MORRIS[†], PRASANTH B. NAIR[*], AND MASAYUKI YANO[*]

**Abstract.** We present a non-intrusive approach to robust structural topology optimization. Specifically, we consider optimization of mean- and variance-based robustness metrics of a linear functional output associated with the linear elasticity equation in the presence of probabilistic uncertainties in the loading and material properties. To provide an efficient approximation of higher-dimensional problems, we approximate the solution to the governing stochastic partial differential equations using the anchored ANOVA Petrov-Galerkin (AAPG) projection scheme. We then develop a non-intrusive quadrature-based formulation to evaluate the robustness metric and the associated shape derivative. The formulation is non-intrusive in the sense that it works with any level-set-based topology optimization code that can provide deterministic displacements, outputs, and shape derivatives for selected stochastic parameter values. We demonstrate the effectiveness of the proposed approach on various problems under loading and material uncertainties.

**Key words.** topology optimization, level-set methods, stochastic elasticity equations, polynomial chaos expansions, stochastic Galerkin projection schemes, anchored ANOVA decompositions

**AMS subject classifications.** 35R60, 60H35, 74P15

## 1. Introduction.

Topology optimization (TO) is a powerful design tool that enables the discovery of unconventional high-performance structures [42, 13]. Unlike size and shape optimization approaches that work with finite-dimensional geometry parametrizations, TO algorithms can, in principle, find an optimal design in an infinite-dimensional space of possible geometries. However, most TO formulations optimize the design under ideal deterministic conditions: i.e., under the assumption that we have precise knowledge of loading conditions and material properties and the fabrication process do not introduce any material or geometric imperfections. The structure optimized under the implicit assumption of determinism may not perform well in the presence of (arguably inevitable) real-world uncertainties [54]. In this work, we develop an approach to robust structural TO that accounts for loading and material uncertainties, is computationally efficient, and is non-intrusive.

Uncertainties encountered in structural TO can be broadly categorized as (i) loading uncertainty, (ii) material uncertainty, (iii) geometric uncertainty, and (iv) model-structure uncertainty. Uncertainties in loading conditions arise from either incomplete knowledge or random fluctuations in the in-service operating environment. Uncertainties in material properties and geometry can be attributed to the manufacturing process used to fabricate the optimal design; e.g., additive manufacturing processes produce stochastic variability in the material due to random spatial fluctuations in the grain size, distributions, and defects. Model-structure uncertainty arises from the use of an idealized mathematical model to predict the performance of candidate designs; e.g., the use of a linear elasticity model even though real strains are never infinitesimal and real stress-strain relationships are never truly linear. The precise

[*]University of Toronto Institute for Aerospace Studies, 4925 Dufferin Street, Ontario, M3H 5T6, Canada (c.audouze@utoronto.ca, aaron.klein@mail.utoronto.ca, pbn@utias.utoronto.ca, masa.yano@utoronto.ca).

[†]Autodesk Research, 661 University Avenue, Toronto, Ontario, M5G 1M1, Canada (adrian.butscher@autodesk.com, nigel.morris@autodesk.com).

mathematical modeling/characterization of these real-world uncertainties is a challenge in itself [44]; however, this is not in the scope of the present work, and we *assume* that we are given a probabilistic model of input uncertainties. We do however recognize that a large number of random variables are required to characterize real-world uncertainties, which demands the development of computationally efficient and scalable robust TO algorithms.

Over the last two decades, robust TO problems have been studied by various researchers. We first review works based on the density-based solid isotropic material with penalization (SIMP) method. Many of the early studies [15, 21, 23, 24, 37, 5] adopted a reliability-based design view point; however, reliability-based methods can be highly sensitive to uncertainty modeling assumptions, and hence the methods may be ill-suited for scenarios with limited experimental/real-world data. More recently, several works have adopted probabilistic metrics to solve robust TO problems using various techniques. Problems considered include robust TO under uncertain loading conditions and locations [19], compliance minimization under multiple uncertain loads [56], compliance minimization under geometric uncertainties [20], and problems where both the objective function and the distribution of the random parameters depend on the design variables [27]. Techniques developed include stochastic Galerkin projection scheme [47], stochastic collocation [30], non-intrusive polynomial chaos (PC) expansions based on sparse grids [22], and a combination of Monte Carlo and stochastic gradient descent [11].

There also exist works on robust TO using boundary variation (or more specifically level-set) methods, which in principle provide a more precise description of geometries than density-based methods. Early work of Conti et al. [10] proposes a two-stage stochastic programming algorithm for TO under loading uncertainties. Dunning et al. [14] similarly consider loading uncertainty and appeal to linearity to recast the robust TO problem as a multi-load TO problem.

Most relevant to the present work are the works based on level-set methods and that consider probabilistic loading and material uncertainties, with a moderate to large number of random variables. As is well known, computationally tractable solutions of such problems require algorithms that mitigate the so-called curse of dimensionality. Chen et al. develop an approach based on univariate dimension-reduction (UDR) combined with numerical quadrature to carry out robust TO under loading and material uncertainties [9] and geometric uncertainties [8]. The UDR approach, unlike multi-variate PC, scales well with the number of random variables. The approach is also non-intrusive and leverages existing (deterministic) analysis and sensitivity analysis codes. However, the UDR approach is limited to a class of problems where the objective function can be well approximated by a sum of one-dimensional functions. Allaire et al. [2] develop an approach based on perturbation methods to approximate robust TO problems under loading, material, and geometric uncertainties. The perturbation method based on Taylor series scales well to high dimensions; however, the approach is limited to small parametric variations. Martínez-Frutos et al. [35] develop an approach based on dimension-adaptive sparse grid to solve robust TO problems under loading and material uncertainties. They also prove the existence of solutions for a class of robust TO problems. However, sparse grids have limited scalability and restrict the applicability of this approach to problems with moderate dimensionality. While the above works have advanced the state-of-the-art in robust TO under realistic loading and material uncertainties that necessitates high-dimensional and large parametric variabilities, further progress is required.

In this work, we present a scalable robust TO algorithm for robustness metrics of linear functional outputs under probabilistic loading and material uncertainties. The contributions of this work are threefold. First, we develop a robust TO framework based on the AAPG projection scheme [4] to efficiently tackle problems with a large number of random variables and large parametric variabilities. Second, we develop a quadrature-based formulation to evaluate the robustness metric and associated shape derivatives; the formulation is non-intrusive in the sense that it can be implemented with any level-set TO codebase that provides deterministic displacements, outputs, and shape derivatives for a given set of loading conditions and materials properties. Third, we demonstrate the effectiveness of the proposed approach by means of numerical studies on TO problems under loading and material uncertainties.

The remainder of this paper is organized as follows. In Section 2, we introduce the robust level-set optimization problem. In Section 3, we formulate the AAPG scheme for the governing linear elasticity SPDEs. In Section 4, we present a minimally intrusive approach for computing the shape derivatives, which leverages existing deterministic TO implementations. In Section 5, we assess the formulation developed using robust optimization problems under loading and material uncertainties.

**2. Notations and problem statement.** Let $\mathcal{D} \in \mathbb{R}^d$ be a bounded working domain ($d \in \{2,3\}$) which contains all the admissible shapes $\Omega \subset \mathcal{D}$. In TO based on level-set methods, the boundary of $\Omega$ denoted by $\partial\Omega$ is defined implicitly with a level-set function $\psi : \mathcal{D} \to \mathbb{R}$ such that $\Omega = \{x \in \mathcal{D} \mid \psi(x) < 0\}$. In this work, we consider randomly parametrized objective functionals of the form

$$J(u(\cdot,\xi),\Omega,\xi) = \int_\Omega j_v(x,\xi)\cdot u(x,\xi)dx + \int_{\partial\Omega_N} j_s(s,\xi)\cdot u(s,\xi)ds, \tag{2.1}$$

where $x \in \Omega$ denotes spatial coordinates and $\xi = (\xi_1,\dots,\xi_M)$ is a $M$-dimensional vector of independent and identically distributed random variables with known joint probability density function $\rho(\xi) = \prod_{i=1}^M \rho_i(\xi_i)$ and joint image $\Gamma = \Gamma_1 \times \cdots \times \Gamma_M \subset \mathbb{R}^M$. We assume the output functions $j_v$ and $j_s$ are linear in the random variables; we will specify the functions in Section 4. The displacement field $u : \Omega \times \Gamma \to \mathbb{R}^d$ is the solution of the random elasticity problem

$$\begin{cases} -\mathrm{div}\big(A(x,\xi)e(u(x,\xi))\big) & = f(x,\xi) & \forall (x,\xi) \in \Omega\times\Gamma, \\ u(x,\xi) & = 0 & \forall (x,\xi) \in \partial\Omega_D\times\Gamma, \\ A(x,\xi)e(u(x,\xi))\,n & = g(x,\xi) & \forall (x,\xi) \in \partial\Omega_N\times\Gamma, \end{cases} \tag{2.2}$$

where $f : \Omega\times\Gamma \to \mathbb{R}^d$ is the body force, $g : \partial\Omega_N\times\Gamma \to \mathbb{R}^d$ is the traction force, $e(u) = \frac{1}{2}(\nabla u + \nabla u^T) : \Omega\times\Gamma \to \mathbb{R}^{d\times d}$ is the strain tensor field, $Ae(u) : \Omega\times\Gamma \to \mathbb{R}^{d\times d}$ is the stress tensor field, $n$ is the outward pointing normal on $\partial\Omega$, and $\partial\Omega_D \neq \emptyset$. We assume that material constitutive properties are described by a random tensor $A(x,\xi) : \mathbb{R}^{d\times d} \to \mathbb{R}^{d\times d}$. Hence, randomness in (2.2) arises from uncertainties in the material properties and/or the loading conditions. In this work, we consider general (possibly nonlinear) material parametrizations with respect to the random variables. To illustrate, an example of parametrization of material properties based on the KL decomposition scheme [32] is provided in Appendix A. Finally, we note that $u$ depends on $\Omega$, even if this dependency is not explicitly indicated.

We next focus on the weak formulation of the random elasticity model. Let $H^1_E(\Omega)^d = \big\{v \in H^1(\Omega)^d \mid v = 0 \text{ on } \partial\Omega_D\big\}$, where $H^1(\Omega)$ is the space of functions over $\Omega$ whose weak first derivative is square integrable. The stochastic weak form of (2.2)

is as follows: find $u \in U = H^1_E(\Omega)^d \otimes L^2(\Gamma)^d$ such that

$$\mathcal{A}(u,v) = \mathcal{B}(v) \quad \forall v \in U, \tag{2.3}$$

where

$$\mathcal{A}(u,v) = \int_\Gamma \int_\Omega A(x,\xi) e(u(x,\xi)) : e(v(x,\xi)) \rho(\xi)\, dx d\xi, \tag{2.4}$$

$$\mathcal{B}(v) = \int_\Gamma \int_\Omega f(x,\xi) \cdot v(x,\xi)\, \rho(\xi)\, dx d\xi + \int_\Gamma \int_{\partial\Omega_N} g(s,\xi) \cdot v(s,\xi)\, \rho(\xi)\, ds d\xi, \tag{2.5}$$

where $A : B$ denotes the Frobenius inner product of tensors $A$ and $B$, and $L^2(\Gamma)$ is the space of square integral functions over $\Gamma$. If the randomness arises exclusively from the loading conditions, the well-posedness of the weak problem can be proved using the Lax-Milgram theorem [6] since the bilinear form $\mathcal{A} : U \times U \to \mathbb{R}$ is continuous and coercive and the linear form $\mathcal{B} : U \to \mathbb{R}$ is continuous. In the presence of material uncertainties, additional assumptions are required (e.g. see [35] in the case of isotropic materials).

REMARK 1. *An example of output functional widely used in TO is the compliance, which we obtain by setting $j_v = f$ and $j_s = g$ so that*

$$J(u(\cdot,\xi),\Omega,\xi) \quad = \quad \int_\Omega f(x,\xi) \cdot u(x,\xi) dx + \int_{\partial\Omega_N} g(s,\xi) \cdot u(s,\xi) ds. \tag{2.6}$$

In this paper, we consider TO problems of the form

$$\begin{aligned} \Omega^* = &\arg \min_{\Omega \subset \mathcal{D}} \mathcal{J}^R(u,\Omega) \\ &\text{subject to } V(\Omega) \le V_{\text{req}} \end{aligned} \tag{2.7}$$

where $\mathcal{J}^R$ is a robustness metric, $V(\Omega) = \int_\Omega dx$ is the volume of $\Omega$, and $V_{\text{req}}$ is a fixed volume parameter. We consider robustness metrics of the form

$$\mathcal{J}^R(u,\Omega) := \mu_J(u,\Omega) + \beta\, \sigma_J(u,\Omega), \tag{2.8}$$

where $\mu_J(u,\Omega)$ and $\sigma_J(u,\Omega)$ are the mean and standard deviation of $J$ defined by

$$\mu_J(u,\Omega) \quad = \quad \langle J(u,\Omega,\cdot)\rangle_\Gamma = \int_\Gamma J(u(\cdot,\xi),\Omega,\xi)\rho(\xi) d\xi, \tag{2.9}$$

$$\sigma_J(u,\Omega) \quad = \quad \langle \big(J(u,\Omega,\cdot) - \mu_J(u,\Omega)\big)^2 \rangle_\Gamma^{1/2}, \tag{2.10}$$

and $\beta \ge 0$ is a user-defined weighting parameter. In addition to the notation $\langle\cdot\rangle_\Gamma$, we will sometimes use one-dimensional average operators defined as $\langle w\rangle_{\Gamma_i} := \int_{\Gamma_i} w\, \rho_i(\xi_i) d\xi_i,\ i = 1,\dots,M$.

In order to satisfy the volume constraint in the optimization problem (2.7) in practice, we use an augmented Lagrangian method, where we enforce the volume constraint by augmenting the objective function as

$$\mathcal{J}(u,\Omega) := \mu_J(u,\Omega) + \beta\, \sigma_J(u,\Omega) + \ell \left(V(\Omega) - V_{\text{req}}\right) + \frac{1}{2\Lambda} \left(V(\Omega) - V_{\text{req}}\right)^2. \tag{2.11}$$

The parameters $\ell$ and $\Lambda$ are updated at every iteration to ensure that the volume constraint $V(\Omega) \le V_{\text{req}}$ is satisfied at the end of the optimization process. We note

that the objective function shares the same structure as the objective function augmented by a fixed volume penalty parameter, which is often used in level-set topology optimization.

We solve the optimization problem (2.7) using a gradient descent algorithm. In level-set methods, the boundary of $\Omega$ is evolved using an advection equation $\frac{\partial \psi}{\partial t} + \theta^* \cdot \nabla \psi = 0$ for the level-set function $\psi : \mathcal{D} \to \mathbb{R}$, where $\theta^* : \mathcal{D} \to \mathbb{R}^d$ is a descent direction that depends on the so-called shape derivative $D_\Omega(\mathcal{J}^R)(u, \cdot)$. There are essentially two types of shape derivatives used in TO, namely boundary-based and distributed, that we briefly introduce in the classical deterministic case. For a given output functional $F$ and any deformation field $\theta \in W^{1,\infty}(\mathbb{R}^d, \mathbb{R}^d)$, classical boundary-based shape derivatives [3] write as $D_\Omega F(u, \Omega)(\theta) = \int_{\partial\Omega} V\, \theta \cdot n \, ds$, where the normal velocity $V$ depends on the state solution $u$ (and possibly of an adjoint solution). The descent direction is thus taken as $\theta^* = -V^{\text{ext}} n$, where $V^{\text{ext}}$ is an extension of $V$ (defined on $\Omega$) to the whole domain $\mathcal{D}$ obtained by using the ersatz material method [3] or any other velocity extension technique (e.g. [1, 48]). On the other hand, distributed shape derivatives introduced more recently by Laurain [28] take the form $D_\Omega F(u, \Omega)(\theta) = \int_\Omega \big(S_1 : D\theta + S_0 \cdot \theta\big) dx$. A smoothed descent direction $\theta^* \in \mathcal{V}(\mathcal{D}) = \big\{\theta \in H^1(\mathcal{D})^d \mid \theta \cdot n = 0 \text{ on } \partial\mathcal{D}\big\}$ is then obtained by solving the equation $\int_\mathcal{D} \big(\alpha_1 D\theta^* : Dw + \alpha_2 \theta^* \cdot w\big) dx = -D_\Omega F(u, \Omega)(w),\ \forall w \in \mathcal{V}(\mathcal{D})$ [12, 28]. We also refer to [43, 46, 29, 25] for more details about theoretical aspects of shape derivatives.

Before providing our robust TO formulation, we make a key assumption motivated by practical considerations according to which a deterministic level-set TO framework is available to the user.

ASSUMPTION 1. *For any given parameter $\xi \in \Gamma$, the quantities required to perform a deterministic TO — the stiffness matrix and load vectors for the finite element analysis, the shape derivatives, and a level-set propagation scheme — are provided.*

Based on this, our goal is to derive a non-intrusive robust TO formulation that leverages any deterministic TO implementation and applies to any randomly parametrized TO problem. We describe in Section 3 a non-intrusive numerical method for solving random elasticity equations with an arbitrary parameterization. A non-intrusive robust TO approach will be presented subsequently in Section 4.

**3. AAPG scheme for random elasticity equations.** In real-world applications, the existence of various sources of uncertainties often necessitates random elasticity equations (2.2) with a large number of parameters. For instance, an accurate description of random fields with a small correlation length can require KL expansions [32] with large numbers of random variables. A classical approach to solve randomly parametrized PDEs is stochastic projection (or gPC) schemes based on PC expansions; see, e.g., [17, 26, 31, 51, 33, 36, 50]. The gPC schemes have been applied successfully to a wide range of stochastic models, including fluid flow or heat transfer problems. The error analysis of gPC approximations of stochastic PDEs are also well established. However, the main limitation of gPC schemes is its computational cost, which becomes prohibitive for problems with large numbers of random variables. Indeed, the number of coupled deterministic PDEs arising from stochastic Galerkin projection increases exponentially with the number of random variables and the PC order. One objective of the present work is to address this limitation (often referred to as the *curse of dimensionality*) by means of an efficient numerical scheme described below.

**3.1. Description of the algorithm.** We propose to solve the random elasticity equations (2.2) using the AAPG scheme [4], which was originally developed to efficiently solve high-dimensional elliptic and parabolic SPDEs. In short, the AAPG scheme decouples high-dimensional stochastic weak forms (such as (2.3)) into low-dimensional stochastic subproblems that can be solved independently of each other. Other approaches based on functional ANOVA decompositions have been studied by several researchers; see [40, 52, 53].

More specifically, consider an anchored ANOVA decomposition for the random elasticity solution

$$u(x,\xi) \simeq \widehat{u}^L(x,\xi) = u^0(x) + \sum_{s=1}^{L} \sum_{j_1<\cdots<j_s} u^{j_1\cdots j_s}(x,\xi_{j_1},\ldots,\xi_{j_s}), \tag{3.1}$$

where $1 \leq L \leq M$. To ensure the uniqueness of the above decomposition, we impose the following null integral contraints on the component functions [40, 18]

$$\int_{\Gamma_k} u^{j_1\cdots j_s}(x,\xi_{j_1},\ldots,\xi_{j_s})\, d\mu_k(\xi_k) = 0 \quad \forall k \in \{j_1,\ldots,j_s\} \tag{3.2}$$

with respect to the Dirac product measure $d\mu(\xi) = \prod_{j=1}^{M} \delta(\xi_j - \xi_j^a) d\xi_j$ , where $\xi^a \in \Gamma$ is a so-called anchor point*. The zero-order component function $u^0$ captures the solution at the anchor point $\xi^a$, the first-order component function $u^{j_1}$ represents the contribution to the solution by the variable $\xi_{j_1}$ acting alone, the second-order component function $u^{j_1 j_2}$ represents the contribution to the solution by the two variables $\xi_{j_1}$ and $\xi_{j_2}$, and so on. By considering a $L$-th order ANOVA decomposition (3.1) with null integral constraints (3.2) with respect to the Dirac product measure along with specially designed test-functions in the high-dimensional weak form (2.3), it can be shown [4] that $u^0$ is the solution of the deterministic elasticity problem

$$\begin{cases} -\mathrm{div}\big(A(x,\xi^a)e(u^0(x))\big) &= f(x,\xi^a) \qquad \forall x \in \Omega, \\ u^0(x) &= 0 \qquad \forall x \in \partial\Omega_D, \\ A(x,\xi^a)e(u^0(x))\, n &= g(x,\xi^a) \qquad \forall x \in \partial\Omega_N. \end{cases} \tag{3.3}$$

In addition, each auxiliary function

$$\widetilde{u}^{j_1}(x,\xi_{j_1}) = u^{j_1}(x,\xi_{j_1}) + u_0(x) \tag{3.4}$$

is the solution of the random elasticity equation (with one random variable)

$$\begin{cases} -\mathrm{div}\big(A(x,\xi^a_{\setminus j_1})e(\widetilde{u}^{j_1}(x,\xi_{j_1}))\big) &= f(x,\xi^a_{\setminus j_1}) \qquad \forall (x,\xi_{j_1}) \in \Omega \times \Gamma_{j_1}, \\ \widetilde{u}^{j_1}(x,\xi_{j_1}) &= 0 \qquad \forall (x,\xi_{j_1}) \in \partial\Omega_D \times \Gamma_{j_1}, \\ A(x,\xi^a_{\setminus j_1})e(\widetilde{u}^{j_1}(x,\xi_{j_1}))\, n &= g(x,\xi^a_{\setminus j_1}) \qquad \forall (x,\xi_{j_1}) \in \partial\Omega_N \times \Gamma_{j_1}, \end{cases} \tag{3.5}$$

where $\xi^a_{\setminus j_1} = (\xi^a_1,\ldots,\xi^a_{j_1-1},\xi_{j_1},\xi^a_{j_1+1},\ldots,\xi^a_M)$. Similarly, each auxiliary function

$$\widetilde{u}^{j_1 j_2}(x,\xi_{j_1},\xi_{j_2}) = u^0(x) + u^{j_1}(x,\xi_{j_1}) + u^{j_2}(x,\xi_{j_2}) + u^{j_1 j_2}(x,\xi_{j_1},\xi_{j_2}) \tag{3.6}$$

is the solution of the random elasticity equation (with two random variables)

$$\begin{cases} -\mathrm{div}\big(A(x,\xi^a_{\setminus j_1 j_2})e(\widetilde{u}^{j_1 j_2}(x,\xi_{j_1},\xi_{j_2}))\big) &= f(x,\xi^a_{\setminus j_1 j_2}) \quad \forall (x,\xi_{j_1},\xi_{j_2}) \in \Omega \times \Gamma_{j_1 j_2}, \\ \widetilde{u}^{j_1 j_2}(x,\xi_{j_1},\xi_{j_2}) &= 0 \quad \forall (x,\xi_{j_1},\xi_{j_2}) \in \partial\Omega_D \times \Gamma_{j_1 j_2}, \\ A(x,\xi^a_{\setminus j_1 j_2})e(\widetilde{u}^{j_1 j_2}(x,\xi_{j_1},\xi_{j_2}))\, n &= g(x,\xi^a_{\setminus j_1 j_2}) \quad \forall (x,\xi_{j_1},\xi_{j_2}) \in \partial\Omega_N \times \Gamma_{j_1 j_2}, \end{cases} \tag{3.7}$$

*A common choice is to take $\xi^a$ as the centroid of $\Gamma$.

where $\Gamma_{j_1 j_2} = \Gamma_{j_1} \times \Gamma_{j_2}$, $\xi^a_{\setminus j_1 j_2} = (\xi^a_1, \dots, \xi^a_{j_1-1}, \xi_{j_1}, \xi^a_{j_1+1}, \dots, \xi^a_{j_2-1}, \xi_{j_2}, \xi^a_{j_2+1}, \dots \xi^a_M)$, and so on for higher-order component functions. See [4] for the derivation.

**3.2. Computational advantages.** We now discuss the computational advantages provided by the AAPG formulation. As a reminder, consider the classical full gPC scheme [17, 51] applied to the original SPDE (2.2). The solution is approximated by $\widehat{u}(x,\xi) = \sum_{k=1}^{N_\xi} u_k(x)\psi_k(\xi)$, where $u_k(x)$ are undetermined spatial functions, $\{\psi_k(\xi)\}_{k=1}^{N_\xi}$ is an orthonormal PC basis, and $N_\xi = \frac{(M+p_\xi)!}{M!p_\xi!}$ is the dimension of the PC basis. Stochastic Galerkin projection yields $N_\xi$ coupled deterministic PDEs

$$\begin{aligned} -\sum_{k=1}^{N_\xi} \operatorname{div}\big(\langle\psi_k\psi_l A(x,\cdot)\rangle_\Gamma\, e(u_k(x))\big) &= \langle f(x,\cdot)\psi_l\rangle_\Gamma \quad \forall x \in \Omega, \quad l = 1,\dots,N_\xi, \\ u_l(x) &= 0 \quad \forall x \in \partial\Omega_D, \quad l = 1,\dots,N_\xi, \\ \sum_{k=1}^{N_\xi} \langle\psi_k\psi_l A(x,\cdot)\rangle_\Gamma\, e(u_k(x))n &= \langle g(x,\cdot)\psi_l\rangle_\Gamma \quad \forall x \in \partial\Omega_N, \quad l = 1,\dots,N_\xi. \end{aligned} \tag{3.8}$$

By contrast, the AAPG scheme requires solving a deterministic elasticity equation for the zeroth-order ANOVA component function $u^0$ and stochastic elasticity problems with $s$ random variables for the higher-order ANOVA component functions $\widetilde{u}^{j_1\cdots j_s}$, $s = 1,\dots,L$. For SPDEs whose solution has a low effective dimension, it is well known that truncated ANOVA decompositions with small truncation orders $L$ are able to represent high-dimensional problems for a wide range of applications while considering low-order interactions[†]. Hence, the stochastic AAPG subproblems are low-dimensional and can be solved efficiently using classical gPC schemes [17, 51]. To be more specific, a second-order AAPG scheme (i.e. with $L = 2$) requires solving one deterministic PDE (3.3), $M$ SPDEs (3.5) each with one random variable, and $\frac{M(M-1)}{2}$ SPDEs (3.7) each with two random variables. If the stochastic AAPG subproblems are solved with gPC schemes, $1 + MN_\xi^{(1)} + \frac{M(M-1)}{2}N_\xi^{(2)}$ deterministic PDEs need to be solved in the end, where $N_\xi^{(1)} = p_\xi + 1$ and $N_\xi^{(2)} = \frac{1}{2}(p_\xi+2)(p_\xi+1)$ are dimensions of PC bases with one and two random variables, $p_\xi$ denoting the PC order. In summary, first- and second-order AAPG schemes scales linearly and quadratically, respectively, with $M$, while a full gPC scheme scales exponentially with $M$.

A major practical advantage of the AAPG formulation is that it is straightforward to parallelize since the AAPG subproblems are independent of each other. In addition, combining AAPG with adaptivity strategies based on Sobol sensitivities (e.g. [53]) allows us to discard random variables that do not contribute much to the solution and consequently it is possible to tackle higher-dimensional stochastic problems. For instance, the combination of AAPG with adaptivity techniques has been shown to efficiently solve large-scale stochastic diffusion problems with around $M = 700$ random variables [38], which would be intractable using a full gPC scheme.

Finally, the AAPG formulation is supported by an *a priori* error analysis. Error estimates that depend on the spatial and stochastic discretization parameters as well as the ANOVA truncation order are provided for time-dependent SPDEs in [4]. The error estimate also informs the choice of an anchor point $\xi^a \in \Gamma$, as we summarize in the following remark.

REMARK 2. *The AAPG error depends on the choice of the anchor point $\xi^a \in \Gamma$, which affects the accuracy of anchored ANOVA decompositions [16, 55]. As discussed in [4], there is an optimal anchor point that minimizes the error $\|u - \hat{u}^L\|_{H^1(\Omega)\otimes L^2(\Gamma)}$*

[†]For example, it is sufficient to consider $L = 2$ in many statistical applications, $L \leq 4$ in molecular dynamics, or $5 \leq L \leq 7$ in data mining (for more details see [18]).

*for each $L$. For the $L = 0$ AAPG approximation, the optimal anchor point is the point that satisfies $u(x,\xi^a) \approx \langle u(x,\xi)\rangle_\Gamma$, and such a point, in principle, may be approximated using a Monte Carlo estimate of $\langle u(x,\xi)\rangle_\Gamma$. However, for $L \geq 1$ AAPG approximations, optimizing the anchor point $\xi^a$ requires the construction of many AAPG estimates $\hat{u}^L$ for various $\xi^a$, which, to the best of our knowledge, cannot be efficiently performed. Hence, we in practice forgo the direct minimization of the error $\|u - \hat{u}^L\|_{H^1(\Omega)\otimes L^2(\Gamma)}$ and instead minimize an a priori error bound in [4]. The error bound, which is based on Taylor series expansion, is minimized when $\xi^a$ is the centroid of $\Gamma$; i.e., $\xi^a = \langle\xi\rangle_\Gamma$.*

**3.3. Solving the AAPG subproblems non-intrusively.** In this section, we focus on the practical resolution of AAPG subproblems based on a semi-discrete spatial finite element (FE) formulation. For a FE discretization of $\Omega$ with a total of $N_x$ spatial dofs, the elasticity equations write as a random linear system $K(\xi)U(\xi) = F(\xi)$, where $K(\xi) \in \mathbb{R}^{N_x\times N_x}$, $F(\xi) \in \mathbb{R}^{N_x}$ and $U(\xi) \in \mathbb{R}^{N_x}$ denote the global stiffness matrix, force vector, and displacement vector, respectively. Next, we focus on the semi-discrete form of the AAPG subproblems. Since the zero-order AAPG subproblem depends on the material property tensor $A(x,\xi^a)$, the semi-discrete form of (3.3) is the deterministic $N_x \times N_x$ linear system $K(\xi^a)U^0 = F(\xi^a)$. Similarly, the semi-discrete forms of the first- and second-order AAPG subproblems (3.5) and (3.7) write as $N_x \times N_x$ random linear systems

$$K(\xi^a_{\setminus j_1})\widetilde{U}^{j_1}(\xi_{j_1}) = F(\xi^a_{\setminus j_1}),\ \forall \xi_{j_1} \in \Gamma_{j_1},\ j_1 = 1,\dots,M, \tag{3.9}$$

$$K(\xi^a_{\setminus j_1 j_2})\widetilde{U}^{j_1 j_2}(\xi_{j_1},\xi_{j_2}) = F(\xi^a_{\setminus j_1 j_2}),\ \forall (\xi_{j_1},\xi_{j_1}) \in \Gamma_{j_1}\times\Gamma_{j_2},\ 1 \leq j_1 < j_2 \leq M. \tag{3.10}$$

The above low-dimensional random matrix equations are solved using gPC schemes. Consider the PC approximation

$$\widetilde{U}^{j_1}(\xi_{j_1}) \simeq \widetilde{U}^{j_1}_{p_\xi}(\xi_{j_1}) = \sum_{l=1}^{N_\xi^{(1)}} \alpha_l^{j_1}\psi_l(\xi_{j_1}), \tag{3.11}$$

where $\{\psi_l\}_{l=1}^{N_\xi^{(1)}}$ is a one-dimensional orthonormal PC basis of total degree $p_\xi$, $\alpha_l^{j_1} \in \mathbb{R}^{N_x}$, and $N_\xi^{(1)} = p_\xi + 1$. In this section, for simplicity, we assume that $p_\xi$ is the same in each stochastic dimension. Enforcing stochastic Galerkin conditions leads to a set of $N_x N_\xi^{(1)} \times N_x N_\xi^{(1)}$ linear systems

$$A^{j_1}\underline{\alpha}^{j_1} = F^{j_1},\ j_1 = 1,\dots,M \tag{3.12}$$

with block matrices

$$A^{j_1} = \begin{pmatrix} B_{11} & \dots & B_{1,N_\xi^{(1)}} \\ \vdots & & \vdots \\ B_{N_\xi^{(1)},1} & \dots & B_{N_\xi^{(1)},N_\xi^{(1)}} \end{pmatrix},\ B_{kl} = \langle\psi_k\psi_l K(\xi^a_{\setminus j_1})\rangle_{\Gamma_{j_1}}, \tag{3.13}$$

solution vector $\underline{\alpha}^{j_1} = (\alpha_1^{j_1},\alpha_2^{j_1},\dots,\alpha_{N_\xi^{(1)}}^{j_1})^T$, and right-hand side $F^{j_1} = (F_1^{j_1},\dots,F_{N_\xi^{(1)}}^{j_1})$, $F_k^{j_1} = \langle\psi_k F(\xi^a_{\setminus j_1})\rangle_{\Gamma_{j_1}}$. Similarly, using PC representations

$$\widetilde{U}^{j_1 j_2}_{p_\xi}(\xi_{j_1},\xi_{j_2}) = \sum_{l=1}^{N_\xi^{(2)}} \alpha_l^{j_1 j_2}\psi_l(\xi_{j_1},\xi_{j_2}) \tag{3.14}$$

with $N_\xi^{(2)} = \frac{1}{2}(p_\xi + 2)(p_\xi + 1)$ and applying stochastic Galerkin conditions leads to $N_x N_\xi^{(2)} \times N_x N_\xi^{(2)}$ linear systems

$$A^{j_1 j_2} \underline{\alpha}^{j_1 j_2} = F^{j_1 j_2},\ 1 \leq j_1 < j_2 \leq M \tag{3.15}$$

with block matrices $B_{kl} = \langle \psi_k \psi_l K(\xi^a_{\setminus j_1 j_2}) \rangle_{\Gamma_{j_1} \times \Gamma_{j_2}}$, and right-hand side components $F_k^{j_1 j_2} = \langle \psi_k F(\xi^a_{\setminus j_1 j_2}) \rangle_{\Gamma_{j_1} \times \Gamma_{j_2}}$.

We now discuss the strategy for solving the set of linear systems (3.12) and (3.15) in practice. The main point to address is an efficient assembly of the block matrices $B_{kl}$ as they depend on $K(\xi)$ which is a general (possibly nonlinear) function of $\xi$. One possible way could be to expand the random stiffness matrix as $K(\xi) \simeq \sum_{m=1}^{N_\xi} K_m \varphi_m(\xi)$, where $\varphi_m(\xi)$ denote $M$-dimensional orthonormal PC basis functions, so that the matrices in (3.12) and (3.15) admit a convenient Kronecker product structure; e.g., $A^{j_1} = \sum_{m=1}^{N_\xi} G_m \otimes K_m$ with $G_m(k,l) = \int_{\Gamma_{j_1}} \psi_k(\xi_{j_1}) \psi_l(\xi_{j_1}) \varphi_m(\xi^a_{\setminus j_1}) \rho_{j_1}(\xi_{j_1}) d\xi_{j_1}$. However, this approach would be computationally expensive since the evaluation of the PC terms $K_m = \langle K(\xi) \varphi_m(\xi) \rangle_\Gamma$ requires the integration of high-dimensional nonlinear functions in the parameter space. Instead, we propose an alternate approach based on a direct computation of the block matrices $B_{kl}$. Since these blocks require only low-dimensional integrals in the parameter space, they can be directly approximated using quadrature rules. For example, the block matrices of $A^{j_1}$ in (3.12) can be computed as

$$B_{kl} \simeq \sum_{i=1}^{N_Q} \omega_{j_1}^{(i)}\, \rho_{j_1}(\xi_{j_1}^{(i)})\, \psi_k(\xi_{j_1}^{(i)})\, \psi_l(\xi_{j_1}^{(i)})\, K(\xi_1^a, \ldots, \xi_{j_1-1}^a, \xi_{j_1}^{(i)}, \xi_{j_1+1}^a, \ldots, \xi_M^a), \tag{3.16}$$

where $(\xi_{j_1}^{(i)}, \omega_{j_1}^{(i)})$ denote quadrature nodes and weights in $\Gamma_{j_1}$.

EXAMPLE 1. *Consider a PC basis of degree $p_\xi$ and assume that $K(\xi)$ is given by a KL expansion [32]. Then the integrands $\psi_k \psi_l K(\xi^a_{\setminus j_1})$ are polynomials of degree $2p_\xi + 1$ in $\xi_{j_1}$, meaning that a Gauss quadrature with $N_Q = p_\xi + 1$ nodes is exact.*

The advantages in using the proposed direct integration approach are two-fold. First, the computational cost is limited since only one- and two-dimensional integrals in the parameter space need to be computed. Second, this technique offers generality as it only requires evaluations of the global stiffness matrix at the parameter points $(\xi_1^a, \ldots, \xi_{j_1-1}^a, \xi_{j_1}^{(i)}, \xi_{j_1+1}^a, \ldots, \xi_M^a)$ and $(\xi_1^a, \ldots, \xi_{j_1-1}^a, \xi_{j_1}^{(i)}, \xi_{j_1+1}^a, \ldots, \xi_{j_2-1}^a, \xi_{j_2}^{(j)}, \xi_{j_2+1}^a, \ldots, \xi_M^a)$. As a result, this non-intrusive approach can treat any type of parametrization for the material properties provided that a black-box uncertainty model is given by the user (i.e., through a function generating evaluations of the global stiffness matrix $K(\xi)$).

**4. Non-intrusive stochastic optimization algorithm.** In this section, we focus on computing shape sensitivities of robustness metrics $\mathcal{J}^R$ defined by (2.8). We assume that $j_v$ and $j_s$ are random functions to address the general case where $\mathcal{J}^R$ explicitly depends on $\xi$.

**4.1. Assumptions and notations.** Before deriving suitable expressions for the shape derivatives of $\mathcal{J}^R$, we state some useful assumptions.

ASSUMPTION 2. *The randomness of the loading conditions are described by $M_L$ random variables $(\xi_1, \ldots, \xi_{M_L})$, and the uncertainties on the material properties are modeled with $M - M_L$ random variables $(\xi_{M_L+1}, \ldots, \xi_M)$. In addition, $\langle \xi_i \rangle_{\Gamma_i} = 0$, $i = 1, \ldots, M_L$.*

Next, we introduce the primal and output linear forms $\mathcal{L}(w,\Omega,\xi) = (f(\cdot,\xi),w)_\Omega + (g(\cdot,\xi),w)_{\partial\Omega_N}$ and $\mathcal{L}_o(w,\Omega,\xi) = (j_v(\cdot,\xi),w)_\Omega + (j_s(\cdot,\xi),w)_{\partial\Omega_N}$, where $(\cdot,\cdot)_\Omega$ and $(\cdot,\cdot)_{\partial\Omega_N}$ denote spatial $L^2$ inner products, and the following assumption:

ASSUMPTION 3. *The loading terms are parametrized linearly in the random variables as* $f(x,\xi) = \overline{\phi}(x) + \sum_{i=1}^M \xi_i\phi_i(x)$ *and* $g(x,\xi) = \overline{\psi}(x) + \sum_{i=1}^M \xi_i\psi_i(x)$, *where* $\phi_i \equiv 0$ *and* $\psi_i \equiv 0$ *for* $i \geq M_L + 1$.

This form of parametrization for the loading terms accommodates many scenarios of interest in engineering applications. For instance, distributed loading terms can be discretized using truncated KL expansions [32] which are commonly used for modeling random fields. The $L^2(\Omega)$-orthogonal functions $\phi_i$ are defined as $\phi_i(x) = \sigma_f\sqrt{\lambda_{f,i}}\widetilde{\phi}_i(x)$, where $\sigma_f$ denotes the standard deviation of the random load $f$ and $\{\lambda_{f,i},\widetilde{\phi}_i\}$ are the eigenpairs of a given two-point correlation function $C_f$ used for modeling $f$. Similar definitions are used for $g$ using $\sigma_g$ and $\{\lambda_{g,i},\widetilde{\psi}_i\}$ for the standard deviation and the eigenpairs of $C_g$, respectively. Furthermore, pointwise loading conditions applied at particular points of the boundary can also be taken into account. For example, two-dimensional parametrizations can be defined by $\overline{\psi}(x) = \sum_{i=1}^{M_L} a_i\delta(x-\overline{x}_i)$ and $\psi_i(x) = \sigma_i a_i^\perp\delta(x-\overline{x}_i)$, where $\overline{x}_i \in \partial\Omega_N$ and $a_i \in \mathbb{R}^d$ are nominal loading vectors. Under Assumption 3, the primal linear form is given by

$$\mathcal{L}(w,\Omega,\xi) = \overline{\mathcal{L}}(w,\Omega) + \sum_{i=1}^M \xi_i\mathcal{L}^i(w,\Omega), \tag{4.1}$$

with

$$\begin{aligned}\overline{\mathcal{L}}(w,\Omega) &= (\overline{\phi},w)_\Omega + (\overline{\psi},w)_{\partial\Omega_N},\\ \mathcal{L}^i(w,\Omega) &= (\phi_i,w)_\Omega + (\psi_i,w)_{\partial\Omega_N}.\end{aligned}$$

We also note that a case with separate decompositions of $f$ and $g$, $f(x,\eta) = \overline{f}(x) + \sum_{j=1}^{M_f}\eta_j f_j(x)$ and $g(x,\zeta) = \overline{g}(x) + \sum_{k=1}^{M_g}\zeta_k g_k(x)$, can be cast in the form in Assumption 3 as follows: $M = M_f + M_g$; $\overline{\phi}(x) = \overline{f}(x)$, $\xi_i = \eta_i$, $\phi_i(x) = f_i(x)$, and $\psi_i(x) = 0$ for $i = 1,\ldots,M_f$; and $\overline{\psi}(x) = \overline{g}(x)$, $\phi_i(x) = 0$, and $\psi_i(x) = g_{i-M_f}(x)$ for $i = M_f+1,\ldots,M_f+M_g$. Multiple independent random fields may be treated using a similar direct decomposition.

Similarly, we make the following assumption on the output form:

ASSUMPTION 4. *The output functions are parametrized linearly in the random variables as* $j_v(x,\xi) = \overline{j}_v(x) + \sum_{i=1}^M \xi_i j_{v,i}(x)\ \ \forall(x,\xi) \in \Omega\times\Gamma$, *and* $j_s(x,\xi) = \overline{j}_s(x) + \sum_{i=1}^M \xi_i j_{s,i}(x)\ \ \forall(x,\xi) \in \partial\Omega_N\times\Gamma$, *where* $j_{v,i} \equiv 0$ *and* $j_{s,i} \equiv 0$ *for* $i \geq M_L + 1$.

As a result, the output linear form is given by

$$\mathcal{L}_o(w,\Omega,\xi) = \overline{\mathcal{L}}_o(w,\Omega) + \sum_{i=1}^M \xi_i\mathcal{L}_o^i(w,\Omega), \tag{4.2}$$

with

$$\begin{aligned}\overline{\mathcal{L}}_o(w,\Omega) &= (\overline{j}_v,w)_\Omega + (\overline{j}_s,w)_{\partial\Omega_N},\\ \mathcal{L}_o^i(w,\Omega) &= (j_{v,i},w)_\Omega + (j_{s,i},w)_{\partial\Omega_N}.\end{aligned}$$

For compliance minimization problems ($j_v = f$ and $j_s = g$), we consider the following additional assumption on the anchor point, which usefulness will be explained in the next section. (See also Remark 2 about the choice of anchor point.)

ASSUMPTION 5. *The anchor point is given by* $\xi^a = \langle\xi\rangle_\Gamma$, *where* $\langle\xi_i\rangle_{\Gamma_i} = 0$, $i = 1,\ldots,M_L$.

**4.2. Shape derivative of statistical moments.** We now derive shape derivatives of statistical moments associated with random elasticity problems with uncertainties in loading conditions and material properties, i.e. with $1 \leq M_L \leq M-1$.

**4.2.1. Shape derivative of the mean.** We first consider the case of general linear output functionals.

PROPOSITION 4.1. *Under Assumptions 2 and 4, the shape derivative of the mean output functional associated with the first-order AAPG approximation of the random elasticity problem (2.2) is given by*

$$D_\Omega\big(\mu_J(u,\Omega)\big) \quad \simeq (1-M) D_\Omega\big(\overline{\mathcal{L}}_o(u^0,\Omega)\big) + \sum_{j_1=1}^{M} \langle D_\Omega\big(\overline{\mathcal{L}}_o(\widetilde{u}^{j_1},\Omega) + \xi_{j_1}\mathcal{L}_o^{j_1}(\widetilde{u}^{j_1},\Omega)\big)\rangle_{\Gamma_{j_1}}. \tag{4.3}$$

*If a second-order AAPG scheme is used, then*

$$\begin{aligned} D_\Omega\big(\mu_J(u,\Omega)\big) \simeq \alpha_M D_\Omega\big(\overline{\mathcal{L}}(u^0,\Omega)\big) + (2-M)\sum_{j_1=1}^{M} \langle D_\Omega\big(\overline{\mathcal{L}}_o(\widetilde{u}^{j_1},\Omega) + \xi_{j_1}\mathcal{L}_o^{j_1}(\widetilde{u}^{j_1},\Omega)\big)\rangle_{\Gamma_{j_1}} \\ + \sum_{j_1<j_2}^{M} \langle D_\Omega\big(\overline{\mathcal{L}}_o(\widetilde{u}^{j_1 j_2},\Omega) + \xi_{j_1}\mathcal{L}_o^{j_1}(\widetilde{u}^{j_1 j_2},\Omega) + \xi_{j_2}\mathcal{L}_o^{j_2}(\widetilde{u}^{j_1 j_2},\Omega)\big)\rangle_{\Gamma_{j_1}\times\Gamma_{j_2}}, \end{aligned} \tag{4.4}$$

*where* $\alpha_M = 1 - M + \frac{1}{2}M(M-1)$ *and* $\sum_{j_1<j_2}^{M}$ *stands for* $\sum_{j_1=1}^{M-1}\sum_{j_2=j_1+1}^{M}$.

*Proof.* Using (3.1) with $L=1$ and (3.4), the AAPG elasticity solution can be rewritten in terms of the auxiliary functions as $\widehat{u}^1(x,\xi) = (1-M)u^0(x) + \sum_{j_1=1}^{M}\widetilde{u}^{j_1}(x,\xi_{j_1})$, from which we obtain

$$\mu_J(u,\Omega) \simeq \langle J(\widehat{u}^1,\Omega,\cdot)\rangle_\Gamma = (1-M)\overline{\mathcal{L}}_o(u^0,\Omega) + \sum_{j_1=1}^{M}\langle\big(\overline{\mathcal{L}}_o(\widetilde{u}^{j_1},\Omega) + \xi_{j_1}\mathcal{L}_o^{j_1}(\widetilde{u}^{j_1},\Omega)\big)\rangle_{\Gamma_{j_1}},$$

from which we deduce (4.3). The expression (4.4) is obtained by rewriting the AAPG elasticity solution as

$$\widehat{u}^2(x,\xi) = \alpha_M u^0(x) + (2-M)\sum_{j_1=1}^{M}\widetilde{u}^{j_1}(x,\xi_{j_1}) + \sum_{j_1<j_2}^{M}\widetilde{u}^{j_1 j_2}(x,\xi_{j_1},\xi_{j_2})$$

using (3.1) with $L=2$, (3.4), and (3.6). ∎

In practice, $\mu_J$ and $D_\Omega(\mu_J)$ are approximated further using PC expansions of total degree $p_\xi$ for the AAPG component functions; i.e. $\widetilde{u}^{j_1} \simeq \widetilde{u}^{j_1}_{p_\xi}$ and $\widetilde{u}^{j_1 j_2} \simeq \widetilde{u}^{j_1 j_2}_{p_\xi}$. (See PC representations (3.11) and (3.14) in a semi-discrete form.) For instance, we estimate the mean of $J$ using one-dimensional quadrature rules in the parameter spaces $\Gamma_{j_1}$:

$$\begin{aligned} \mu_J(u,\Omega) \simeq (1-M)\overline{\mathcal{L}}_o(u^0,\Omega) \\ + \sum_{j_1=1}^{M}\sum_{i=1}^{N_Q}\omega_{j_1}^{(i)}\rho_{j_1}(\xi_{j_1}^{(i)})\big(\overline{\mathcal{L}}_o(\widetilde{u}^{j_1}(\cdot,\xi_{j_1}^{(i)}),\Omega) + \xi_{j_1}^{(i)}\mathcal{L}_o^{j_1}(\widetilde{u}^{j_1}(\cdot,\xi_{j_1}^{(i)}),\Omega)\big). \end{aligned} \tag{4.5}$$

To ensure consistency between the approximations of $\mu_J$ and its shape derivative, we use the same quadrature rules to estimate (4.3) and (4.4). It is worth mentioning that

*deterministic* shape gradients $D_\Omega(\cdot)$ can be evaluated using any method, including the boundary-based [3] and distributed [28] formulations. When approximating (4.3) and (4.4) with quadrature rules, the shape derivatives of the output linear forms $\overline{\mathcal{L}}_o$ and $\mathcal{L}_o^{j_1}$ can be estimated using the classical Céa's optimization method [7, 3]. For example, $D_\Omega\big(\overline{\mathcal{L}}_o(u^0,\Omega)\big) = D_\Omega\big(L(u^0,p^0,\Omega)\big)$, where $L$ is the Lagrangian defined as

$$\begin{aligned} L(v,q,\Omega) \quad &:= \int_\Omega \overline{j}_v \cdot v + \int_{\partial\Omega_N} \overline{j}_s \cdot v + \int_\Omega A(x,\xi^a)e(v) : e(q) - \int_\Omega f(x,\xi^a)\cdot q \\ &\quad - \int_{\partial\Omega_N} g(x,\xi^a)\cdot q - \int_{\partial\Omega_D}\big(A(s,\xi^a)e(v)n\cdot q + A(s,\xi^a)e(q)n\cdot v\big) \end{aligned}$$

and $p^0$ is the adjoint state solution of

$$\left\{\begin{array}{rll} -\mathrm{div}\big(A(x,\xi^a)e(p^0(x))\big) & = -\overline{j}_v(x) & \forall x\in\Omega, \\ p^0(x) & = 0 & \forall x\in\partial\Omega_D, \\ A(x,\xi^a)e(p^0(x))\,n & = -\overline{j}_s(x) & \forall x\in\partial\Omega_N. \end{array}\right.$$

The shape gradient $D_\Omega\big(\overline{\mathcal{L}}_o(u^0,\Omega)\big)$ is then obtained by using any type of deterministic shape derivative $D_\Omega\big(L(u^0,p^0,\Omega)\big)$. Overall, estimating $D_\Omega(\cdot)$ in (4.3) requires solving $1+MN_Q$ deterministic adjoint problems; i.e., $1+MN_Q$ deterministic linear systems that depend on the stiffness matrices $K(\xi^a)$ and $K(\xi^a_1,\dots,\xi^a_{j_1-1},\xi^{(i)}_{j_1},\xi^a_{j_1+1},\dots,\xi^a_M)$. Similarly, $1+MN_Q+M(M-1)N_Q^2/2$ deterministic adjoint equations need to be solved to carry out all the shape derivatives in (4.4).

REMARK 3. *By using the same quadrature rule for assembling the block matrices $B_{kl}$ (see (3.16)) and for approximating the integrals in $D_\Omega(\mu_J)$, the stiffness matrices evaluated at the quadrature points in the adjoint problems are the same as those used for assembling the matrices in the primal problems.*

We now focus on the shape derivative of the mean compliance (i.e., $j_v = f$ and $j_s = g$).

PROPOSITION 4.2. *Under Assumptions 2, 3 and 5, the shape derivative of the mean compliance associated with the first-order AAPG approximation of the random elasticity problem (2.2) is given by*

$$D_\Omega\big(\mu_J(u,\Omega)\big) \simeq (1-M)D_\Omega\big(J(u^0,\Omega)\big) + \sum_{j_1=1}^{M}\langle D_\Omega\big(J(\widetilde{u}^{j_1},\Omega,\xi_{j_1})\big)\rangle_{\Gamma_{j_1}}. \tag{4.6}$$

*If a second-order AAPG scheme is used, then*

$$\begin{aligned} D_\Omega\big(\mu_J(u,\Omega)\big) \simeq \alpha_M D_\Omega\big(J(u^0,\Omega)\big) &+ (2-M)\sum_{j_1=1}^{M}\langle D_\Omega\big(J(\widetilde{u}^{j_1},\Omega,\xi_{j_1})\big)\rangle_{\Gamma_{j_1}} \\ &+ \sum_{j_1<j_2}^{M}\langle D_\Omega\big(J(\widetilde{u}^{j_1 j_2},\Omega,\xi_{j_1},\xi_{j_2})\big)\rangle_{\Gamma_{j_1}\times\Gamma_{j_2}}. \end{aligned} \tag{4.7}$$

*Proof.* For a first-order AAPG scheme, the random compliance is given by $J(u,\Omega,\xi) \simeq \mathcal{L}(\widehat{u}^1,\Omega,\xi) = (1-M)\mathcal{L}(u^0,\Omega,\xi) + \sum_{j_1=1}^{M}\mathcal{L}(\widetilde{u}^{j_1},\Omega,\xi)$, which yields

$$\mu_J(u,\Omega) \simeq (1-M)\langle\mathcal{L}(u^0,\Omega,\cdot)\rangle_\Gamma + \sum_{j_1=1}^{M}\langle\mathcal{L}(\widetilde{u}^{j_1},\Omega,\cdot)\rangle_\Gamma. \tag{4.8}$$

By definition of the anchor point (see Assumption 5), it holds $J(u^0,\Omega) = (f(\cdot,\xi^a),u^0)_\Omega + (g(\cdot,\xi^a),u^0)_{\partial\Omega_N} = (\overline{\phi},u^0)_\Omega + (\overline{\psi},u^0)_{\partial\Omega_N} = \overline{\mathcal{L}}(u^0,\Omega)$. Since the $M_L$ first random variables are centered, it follows that

$$\langle \mathcal{L}(u^0,\Omega,\cdot)\rangle_\Gamma = \overline{\mathcal{L}}(u^0,\Omega) = J(u^0,\Omega). \tag{4.9}$$

Next, the first-order AAPG terms can be expressed as

$$\begin{aligned}
\langle \mathcal{L}(\widetilde{u}^{j_1},\Omega,\cdot)\rangle_\Gamma &= \langle \overline{\mathcal{L}}(\widetilde{u}^{j_1},\Omega)\rangle_\Gamma + \sum_{i=1}^{M}\langle \xi_i \mathcal{L}^i(\widetilde{u}^{j_1},\Omega)\rangle_\Gamma \\
&= \begin{cases} \langle (\overline{\phi}+\xi_{j_1}\phi_{j_1},\widetilde{u}^{j_1})_\Omega + (\overline{\psi}+\xi_{j_1}\psi_{j_1},\widetilde{u}^{j_1})_{\partial\Omega_N}\rangle_{\Gamma_{j_1}}, & j_1 = 1,\dots M_L \\ \langle (\overline{\phi},\widetilde{u}^{j_1})_\Omega + (\overline{\psi},\widetilde{u}^{j_1})_{\partial\Omega_N}\rangle_{\Gamma_{j_1}}, & j_1 \geq M_L+1 \end{cases} \\
&= \langle (f(\cdot,\xi^a_{\setminus j_1}),\widetilde{u}^{j_1})_\Omega + (g(\cdot,\xi^a_{\setminus j_1}),\widetilde{u}^{j_1})_{\partial\Omega_N}\rangle_{\Gamma_{j_1}} \\
&= \langle J(\widetilde{u}^{j_1},\Omega,\cdot)\rangle_{\Gamma_{j_1}}.
\end{aligned} \tag{4.10}$$

We deduce (4.6) by combining (4.8), (4.9), and (4.10) and applying the shape derivative. The same arguments are used to obtain (4.7). ∎

In practice, as before, the shape sensitivities of the mean compliance are approximated further using quadrature rules in one- and two-dimensional parameter spaces and PC approximations of AAPG component functions; e.g.,

$$D_\Omega\big(\mu_J(u,\Omega)\big) \simeq (1-M)D_\Omega\big(J(u^0,\Omega)\big) + \sum_{j_1=1}^{M}\sum_{i=1}^{N_Q}\omega_{j_1}^{(i)}\rho_{j_1}(\xi_{j_1}^{(i)})D_\Omega\big(J(\widetilde{u}^{j_1}_{p_\xi},\Omega,\xi_{j_1}^{(i)})\big). \tag{4.11}$$

Remark 4. *As previously mentioned, the proposed approach is minimally intrusive from an implementation point of view. Indeed, the computation of $D_\Omega(\mu_J)$ depends on shape sensitivities of Lagrangian terms in the non-compliant case and on shape sensitivities of $J$ in the compliant case, each of them depending on AAPG component functions evaluated at quadrature points in the parameter space. Any available boundary-based [3] or distributed [28] shape gradient implementation within a deterministic TO library can then be used as a black-box solver to perform all the required deterministic shape gradients for (4.3), (4.4), or (4.11).*

**4.2.2. Shape derivative of the standard deviation.** We now consider shape derivatives of the standard deviation. Since the shape derivative of the standard deviation of $J$ can be expressed as $D_\Omega\big(\sigma_J(u,\Omega)\big) = \frac{1}{2}(\sigma_J^2(u,\Omega))^{-1/2}D_\Omega\big(\sigma_J^2(u,\Omega)\big)$, we derive an expression for the variance $\sigma_J^2(u,\Omega)$ in what follows.

Proposition 4.3. *Under Assumptions 2 and 4, the variance of the output functional associated with the first-order AAPG approximation of the random elasticity problem (2.2) is given by*

$$\begin{aligned}
\sigma_J^2(u,\Omega) \simeq (1-M)^2\sum_{i=1}^{M_L}\langle \xi_i^2\rangle_{\Gamma_i}\mathcal{L}_o^i(u^0,\Omega)^2 + 2(1-M)\sum_{j_1=1}^{M}A_{j_1}(u^0,\widetilde{u}^{j_1},\Omega) \\
+ \sum_{j_1=1}^{M}\sum_{k_1=1}^{M}\big(B_{j_1}(\widetilde{u}^{j_1},\Omega)\delta_{j_1,k_1} + C_{j_1,k_1}(\widetilde{u}^{j_1},\widetilde{u}^{k_1},\Omega)(1-\delta_{j_1,k_1})\big),
\end{aligned} \tag{4.12}$$

*where*

$$A_{j_1}(u^0,\widetilde{u}^{j_1},\Omega) = \mathcal{L}_o^{j_1}(u^0,\Omega)\,\langle \xi_{j_1}\big(\overline{\mathcal{L}}_o(\widetilde{u}^{j_1},\Omega)+\xi_{j_1}\mathcal{L}_o^{j_1}(\widetilde{u}^{j_1},\Omega)\big)\rangle_{\Gamma_{j_1}} + \sum_{i\neq j_1}^{M}\langle\xi_i^2\rangle_{\Gamma_i}\mathcal{L}_o^i(u^0,\Omega)\langle\mathcal{L}_o^i(\widetilde{u}^{j_1},\Omega)\rangle_{\Gamma_{j_1}},$$

$$\begin{aligned}B_{j_1}(\widetilde{u}^{j_1},\Omega) &= \langle\overline{\mathcal{L}}_o(\widetilde{u}^{j_1},\Omega)^2\rangle_{\Gamma_{j_1}} - \langle\overline{\mathcal{L}}_o(\widetilde{u}^{j_1},\Omega)\rangle_{\Gamma_{j_1}}^2 + 2\langle\xi_{j_1}\overline{\mathcal{L}}_o(\widetilde{u}^{j_1},\Omega)\mathcal{L}_o^{j_1}(\widetilde{u}^{j_1},\Omega)\rangle_{\Gamma_{j_1}}\\ &\quad - 2\langle\overline{\mathcal{L}}_o(\widetilde{u}^{j_1},\Omega)\rangle_{\Gamma_{j_1}}\langle\xi_{j_1}\mathcal{L}_o^{j_1}(\widetilde{u}^{j_1},\Omega)\rangle_{\Gamma_{j_1}} + \sum_{i\neq j_1}^{M}\langle\xi_i^2\rangle_{\Gamma_i}\langle\mathcal{L}_o^i(\widetilde{u}^{j_1},\Omega)^2\rangle_{\Gamma_{j_1}}\\ &\quad + \langle\xi_{j_1}^2\mathcal{L}_o^{j_1}(\widetilde{u}^{j_1},\Omega)^2\rangle_{\Gamma_{j_1}} - \langle\xi_{j_1}\mathcal{L}_o^{j_1}(\widetilde{u}^{j_1},\Omega)\rangle_{\Gamma_{j_1}}^2,\end{aligned}$$

$$\begin{aligned}C_{j_1,k_1}(\widetilde{u}^{j_1},\widetilde{u}^{k_1},\Omega) &= \langle\mathcal{L}_o^{k_1}(\widetilde{u}^{j_1},\Omega)\rangle_{\Gamma_{j_1}}\langle\xi_{k_1}\big(\overline{\mathcal{L}}_o(\widetilde{u}^{k_1},\Omega)+\xi_{k_1}\mathcal{L}_o^{k_1}(\widetilde{u}^{k_1},\Omega)\big)\rangle_{\Gamma_{k_1}}\\ &\quad + \langle\xi_{j_1}\big(\overline{\mathcal{L}}_o(\widetilde{u}^{j_1},\Omega)+\xi_{j_1}\mathcal{L}_o^{j_1}(\widetilde{u}^{j_1},\Omega)\big)\rangle_{\Gamma_{j_1}}\langle\mathcal{L}_o^{j_1}(\widetilde{u}^{k_1},\Omega)\rangle_{\Gamma_{k_1}}\\ &\quad + \sum_{i\neq(j_1,k_1)}^{M}\langle\xi_i^2\rangle_{\Gamma_i}\langle\mathcal{L}_o^i(\widetilde{u}^{j_1},\Omega)\rangle_{\Gamma_{j_1}}\langle\mathcal{L}_o^i(\widetilde{u}^{k_1},\Omega)\rangle_{\Gamma_{k_1}}\\ &\quad + \langle\xi_{j_1}\mathcal{L}_o^{k_1}(\widetilde{u}^{j_1},\Omega)\rangle_{\Gamma_{j_1}}\langle\xi_{k_1}\mathcal{L}_o^{j_1}(\widetilde{u}^{k_1},\Omega)\rangle_{\Gamma_{k_1}},\end{aligned}$$

*and $\delta_{ij}$ denotes the Kronecker delta.*

*Proof.* The variance of $J$ is approximated as

$$\begin{aligned}\sigma_J^2(u,\Omega) &\simeq \langle J(\widehat{u}^1,\Omega,\cdot)^2\rangle_\Gamma - \mu_J(\widehat{u}^1,\Omega)^2 = (1-M)^2\big(\langle\mathcal{L}_o(u^0,\Omega)^2\rangle_\Gamma - \overline{\mathcal{L}}_0(u^0,\Omega)^2\big)\\ &\quad + 2(1-M)\sum_{j_1=1}^{M}\big(\langle\mathcal{L}_o(u^0,\Omega)\mathcal{L}_o(\widetilde{u}^{j_1},\Omega)\rangle_\Gamma - \overline{\mathcal{L}}_0(u^0,\Omega)\langle\mathcal{L}_o(\widetilde{u}^{j_1},\Omega)\rangle_\Gamma\big)\\ &\quad + \sum_{j_1=1}^{M}\sum_{k_1=1}^{M}\big(\langle\mathcal{L}_o(\widetilde{u}^{j_1},\Omega)\mathcal{L}_o(\widetilde{u}^{k_1},\Omega)\rangle_\Gamma - \langle\mathcal{L}_o(\widetilde{u}^{j_1},\Omega)\rangle_\Gamma\langle\mathcal{L}_o(\widetilde{u}^{k_1},\Omega)\rangle_\Gamma\big)\end{aligned}\tag{4.13}$$

since $\langle\xi_i\rangle_{\Gamma_i}=0$, $i=1,\dots,M_L$. We obtain (4.12) by expanding each term in (4.13), using the fact that $\mathcal{L}_o^i\equiv 0$ for $i\geq M_L+1$ and that the $M_L$ first random variables are centered. ∎

As a result, the calculation of the shape derivative $D_\Omega\big(\sigma_J^2(\widehat{u}^1,\Omega)\big)$ requires computing the terms $(D_\Omega(\mathcal{L}_o^{j_1}(u^0,\Omega)))_{j_1=1,\dots,M_L}$, $(D_\Omega\big(\overline{\mathcal{L}}_o(\widetilde{u}^{j_1}(\cdot,\xi_{j_1}^{(i)}),\Omega)\big))_{j_1=1,\dots,M}$, and $(D_\Omega\big(\mathcal{L}_o^{j_1}(\widetilde{u}^{k_1}(\cdot,),\Omega)\big))_{j_1=1,\dots,M_L,k_1=1,\dots,M}$, where $(\xi_{j_1}^{(i)})_{i=1,\dots,N_Q}$ denote quadrature nodes used to approximate one-dimensional integrals in $\Gamma_{j_1}$. Hence, computing $D_\Omega\big(\sigma_J^2(\widehat{u}^1,\Omega)\big)$ requires solving $M_L+(1+M_L)MN_Q$ (deterministic) adjoint problems.

We refer to Appendix B for the shape derivative of the variance for compliance minimization problems. In particular, we focus on simplified cases where the randomness is coming exclusively from uncertainties on the material properties ($M_L=0$) or from the loading conditions ($M_L=M$).

**4.3. Comparison with existing approaches.** We conclude the section with a discussion of the comparison between the proposed approach and existing approaches. In [9] the shape derivatives of statistical moments of a random functional are computed using an univariate dimension reduction (UDR) approach; i.e.,

a first-order anchored ANOVA decomposition with anchor point $\xi^a = \langle\xi\rangle$, where $J(u,\Omega,\xi) \simeq (1-M)J(u,\Omega,\xi^a) + \sum_{j_1=1}^{M} J(u,\Omega,\xi^a_{\setminus j_1})$. For example, the shape derivative of the mean of $J$ is computed as

$$D_\Omega\big(\mu_J(u,\Omega)\big) \simeq (1-M)D_\Omega\big(J(u,\Omega,\xi^a)\big) + \sum_{j_1=1}^{M}\sum_{k=1}^{m_{j_1}} \omega_{j_1}^{(k)} D_\Omega\big(J(u,\Omega,\xi_1^a,\dots,\xi_{j_1-1}^a,\xi_{j_1}^{(k)},\xi_{j_1+1}^a,\dots,\xi_M^a)\big)$$

using one-dimensional quadrature rules in the parameter space. This technique is fully non-intrusive since it requires only shape gradients of deterministic state solutions evaluated at the quadrature points. By contrast, the proposed approach is semi-intrusive since it involves shape derivatives of AAPG component functions; see, e.g., (4.3). Even if the UDR approach allows us to handle any type of random functional, its fully non-intrusive feature might be less accurate than the proposed AAPG-based approach. In terms of computational cost, the UDR approach requires $\mathcal{O}\big((1+m_1+\cdots+m_M)N_x\big)$ operations since each deterministic elasticity problem scales in $\mathcal{O}(N_x)$. If sparse grids with level $l$ are used in each dimension, the overall cost is $\mathcal{O}\big((1+M2^l)N_x\big)$. On the other hand, the proposed approach (based on first-order AAPG) requires $\mathcal{O}\big((1+M(p_\xi+1))N_x\big)$ operations for the primal problems since one deterministic elasticity equation and $M$ stochastic elasticity problems with one random variables need to be solved. In the case of non-compliant problems, an additional cost of $\mathcal{O}\big((1+MN_Q)N_x\big)$ operations is required to solve the adjoint problems to compute $D_\Omega(\mu_J)$. As such, both approaches have a similar abstract computational cost (with the coefficient $2^l$ growing faster than $p_\xi+1$ or $p_\xi+1+N_Q$). In comparison to the first-order AAPG and UDR, the second-order AAPG formulation requires $\mathcal{O}((1+M(p_\xi+1)+\frac{M(M-1)}{2}\frac{(p_\xi+2)(p_\xi+1)}{2})N_x)$ operations for the primal problem and $\mathcal{O}((1+MN_Q+\frac{M(M-1)}{2}N_Q^2)N_x)$ operations for the adjoint problems.

The proposed formulation can also be compared with the approach from Martínez-Frutos et al. [35], wherein the shape derivatives of robustness metrics are expressed in terms of integrals over the original parameter space $\Gamma$, and these integrals are subsequently approximated using adaptive sparse quadrature rules. However, this technique can scale poorly for high-dimensional problems. Using sparse grids with level $l$ in the $M$-dimensional parameter space, this approach requires $\mathcal{O}\big(2^l l^{M-1}N_x\big)$ operations at each optimization iteration. By contrast, the proposed AAPG-based formulation breaks down the complexity since shape derivatives of robustness metrics are expressed in terms of low-dimensional integrals in the parameter space. For example, in the compliance case, the cost for the first-order AAPG formulation is $\mathcal{O}\big(M(p_\xi+M_LN_Q)N_x\big)$ per optimization iteration ($\mathcal{O}\big(Mp_\xi N_x\big)$ for primal problems and $\mathcal{O}\big(MM_LN_QN_x\big)$ for adjoint problems), which allows to tackle problems with larger number of random parameters.

**5. Numerical results.** We now present numerical illustrations of the proposed formulation for two-dimensional TO problems under different sources of uncertainties.

**5.1. Loading uncertainties.** In this section we focus on cases where the randomness arises from loading conditions ($M_L = M$). For all examples, we consider isotropic materials with Young's modulus $E = 1$ and Poisson's ratio $\nu = 0.3$. We assume there is no body force ($f \equiv 0$) and that the traction force $g$ admits an affine decomposition of the form discussed in Section 4.1. We minimize the mean compliance (2.9) subject to volume constraints, using an augmented Lagrangian method (2.11).

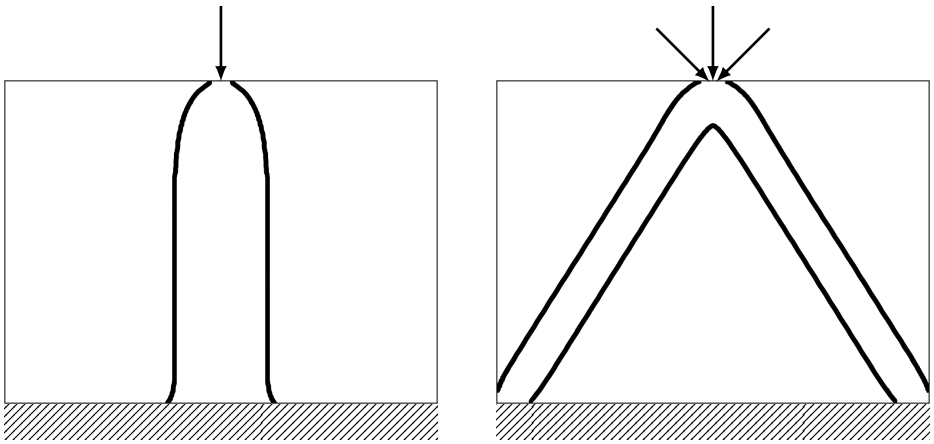

FIG. 5.1. *Vertical column under loading uncertainties:* $\Omega_{\text{det,opt}}$ *(left) and* $\Omega_{\text{stoch,opt}}$ *(right).*

We assume the Dirichlet boundary $\partial\Omega_D$ is fixed and that the Neumann boundary is partitioned into two parts: $\partial\Omega_{N,g}$, over which $g \neq 0$ and is fixed (i.e., non-designable); $\partial\Omega_{N,0}$, over which $g = 0$ and is optimized.

We use the superposition principle described in Appendix B.2, where each component of the displacement field ($u^0$ and $u^i$) and their shape derivatives are computed using an in-house TO solver that builds on the FEniCS library and TO code developed by Laurain [28]. The working domains are discretized using triangular finite elements with linear shape functions.

Starting from the same initial shape we generate two types of optimal designs. The deterministic design $\Omega_{\text{det,opt}}$ is obtained by applying a classical TO solver for minimizing the compliance (i.e., ignoring uncertainties); the stochastic design $\Omega_{\text{stoch,opt}}$ is generated using the mean compliance minimization (i.e., (2.8) with $\beta = 0$). For each optimal design, we compute two performance metrics: the nominal compliance $J_{\text{nom}} := J(u(\cdot, \xi = 0), \Omega, \xi = 0)$ and the mean compliance $\mu_J$, which we compute directly and exactly using the AAPG decomposition.

**5.1.1. Pointwise loading.** We first consider a vertical column problem, initialized with a solid domain with holes removed in a $2 \times 7$ checkerboard pattern. We apply a point random load $g(x, \xi) = \big((0, -1)^T + \xi(1, 0)^T\big)\delta(x - \overline{x})$, where $\overline{x} = (0.5, 1)$ is the middle of the top boundary, and $\xi \sim \mathcal{U}[-1, 1]$. We discretize the square working domain $\mathcal{D} = [0, 1]^2$ using 360,000 elements and set the volume fraction to $V_{\text{req}}/|\mathcal{D}| = 0.2$.

Fig. 5.1 shows the optimized designs. The nominal-optimized design $\Omega_{\text{det,opt}}$ yields a nominal compliance of $J_{\text{nom}} = 6.67$ and a mean compliance of $\mu_J = 128.9$. The mean-optimized design $\Omega_{\text{stoch,opt}}$ yields a nominal compliance of $J_{\text{nom}} = 8.70$ and a mean compliance of $\mu_J = 18.99$. The mean-optimized design slightly sacrifices nominal (i.e., on-design) performance to obtain a substantially better off-design performance, resulting in a better mean compliance. The nominal-optimized design is a single vertical beam, which is ideal for supporting vertical load but not any horizontal loads. The mean-optimized design is triangular to better support horizontal loads.

We next consider a half-wheel problem, initialized with a solid domain with holes removed in a $4 \times 7$ checkerboard pattern. We apply a point random load $g(x, \xi) = \big((0, -1)^T + \xi(1, 0)^T\big)\delta(x - \overline{x})$, where $\overline{x} = (1, 0)$ is the middle of the bottom boundary, and $\xi \sim \mathcal{U}[-1, 1]$. We discretize the rectangular domain $\mathcal{D} = [0, 2] \times [0, 1]$ using 80,000

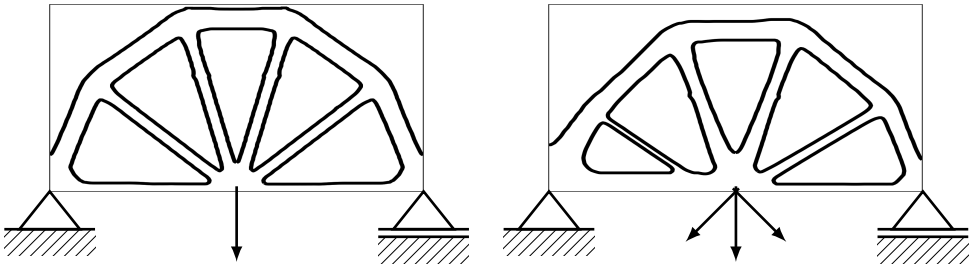

FIG. 5.2. *Half-wheel under loading uncertainties:* $\Omega_{\text{det,opt}}$ *(left) and* $\Omega_{\text{stoch,opt}}$ *(right).*

elements and set the volume fraction to $V_{\text{req}}/|\mathcal{D}| = 0.3$.

Optimized designs are depicted on Fig. 5.2. The nominal-optimized design $\Omega_{\text{det,opt}}$ yields a nominal compliance of $J_{\text{nom}} = 19.83$ and a mean compliance of $\mu_J = 30.37$. The mean-optimized design $\Omega_{\text{stoch,opt}}$ yields a nominal compliance of $J_{\text{nom}} = 20.80$ and a mean compliance of $\mu_J = 27.60$. Again, the mean-optimized design slightly sacrifices the on-design performance to improve the off-design performance. The nominal-optimized design has essentially no horizontal members as the nominal load is purely vertical; the mean-optimized design has a thicker horizontal member to better support horizontal random loads.

**5.1.2. Distributed loading: moderate-dimensional case.** We next consider a carrier plate problem, initialized with a solid domain with holes removed in a $4 \times 5$ checkerboard pattern. We represent the random distributed load on the top boundary using a KL expansion,

$$g(x,\xi) = \begin{pmatrix} 0 \\ \overline{g} \end{pmatrix} + \sum_{m=1}^{M} \xi_m \begin{pmatrix} g_m(x) \\ 0 \end{pmatrix}, \tag{5.1}$$

where $\overline{g} = -1$ is a nominal vertical load amplitude, $\xi_m \sim \mathcal{U}[-1,1]$, $g_m(x) = \sigma_g \sqrt{\lambda}_m \phi_m(x)$, and $\{\lambda_m, \phi_m\}$ are the eigenpairs of a two-point correlation function $C_g(x,y) = \sigma_g^2\, e^{-\frac{||x-y||}{l}}$ with $\sigma_g = 1$ and $l = 5$. We choose $M = 4$, which captures 99% of the energy. We discretize the squared domain $\mathcal{D} = [0,1]^2$ using 250,000 elements and set the volume fraction to $V_{\text{req}}/|\mathcal{D}| = 0.5$.

Fig. 5.3 shows the optimized designs. The nominal-optimized design $\Omega_{\text{det,opt}}$ yields a nominal compliance of $J_{\text{nom}} = 1.9$ and the mean compliance of $\mu_J = 39.4$. The mean-optimized design yields a nominal compliance of $J_{\text{nom}} = 2.6$ and the mean compliance of $\mu_J = 7.23$. The mean-optimized design again sacrifices the nominal performance to obtain a better off-design performance. The mean-optimized design incorporates more diagonal members to better support horizontal loads.

**5.1.3. Distributed loading: higher-dimensional case.** To demonstrate the ability of the AAPG method to handle problems with a larger number of random variables, we again consider the carrier plate problem with the distributed load of the form (5.1) and a two-point correlation function $C_g(x,y) = \sigma_g^2\, e^{-\frac{||x-y||}{l}}$. However, in this case, we consider a shorter correlation length of $l = 2$ and choose $M = 52$ to capture 99.9% of the energy (instead of $l = 5$, $M = 4$, and 99% of captured energy in Section 5.1.2). Fig. 5.4 shows the mean-optimized design, which yields a nominal and mean compliance of $J_{\text{nom}} = 2.6$ and $\mu_J = 7.07$, respectively; the nominal-optimized design yields a nominal and mean compliance of $J_{\text{nom}} = 1.9$ and $\mu_J = 37.8$,

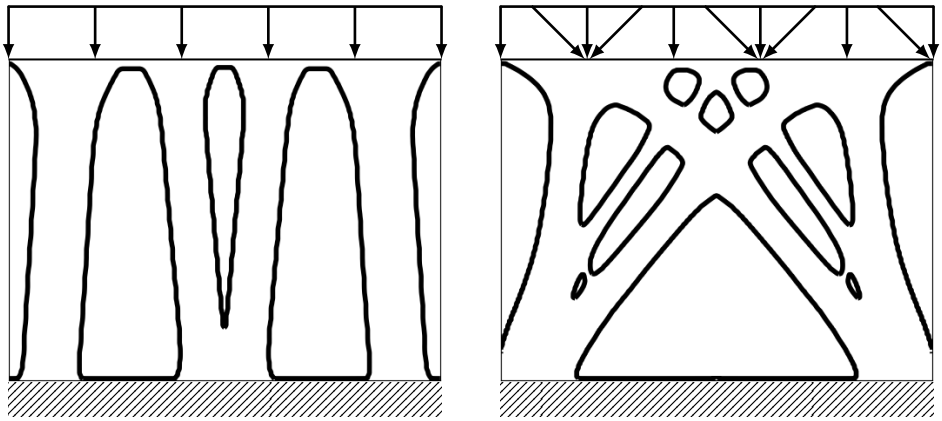

FIG. 5.3. *Carrier plate under moderate-dimensional loading uncertainties with $M = 4$ random variables: $\Omega_{\text{det,opt}}$ (left) and $\Omega_{\text{stoch,opt}}$ (right).*

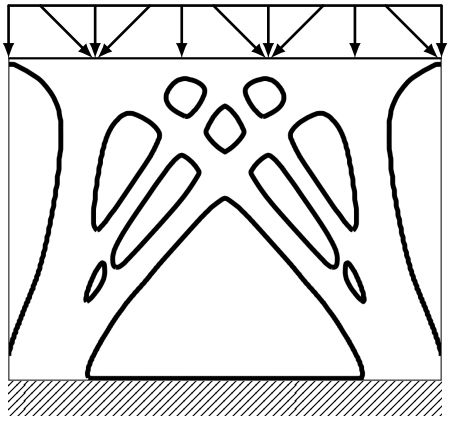

FIG. 5.4. *Carrier plate under higher-dimensional loading uncertainties with $M = 52$ random variables: mean-optimized design $\Omega_{\text{stoch,opt}}$.*

respectively. (As the nominal load is the same as the moderate-dimensional case considered in Section 5.1.2, the nominal-optimized design $\Omega_{\text{det,opt}}$ is the same as that reported in Section 5.1.2; however, $\mu_J$ for the nominal-optimized design is different because the random load is different.) The evaluation of the robustness metric for this higher-dimensional problem requires the solution of $M = 52$ linear systems, but this can be performed efficiently as the systems share the same stiffness matrix. For our current (sequential) implementation, the computational time for this $M = 52$ case is $\approx 2.2$ times the computational time for the $M = 4$ case.

**5.2. Uncertainties in material properties.** We now consider TO under material uncertainties. In all examples, we consider isotropic materials with random Young's modulus field; Poisson's ratio is fixed to $\nu = 0.3$. We assume there is no body force ($f \equiv 0$) and that the traction force $g$ is deterministic ($M_L = 0$). We minimize a weighted sum of the mean and standard deviation of the compliance (2.6) subject to volume constraints, using an augmented Lagrangian method. We assume the Dirichlet boundary $\partial\Omega_D$ is fixed and that the Neumann boundary is partitioned

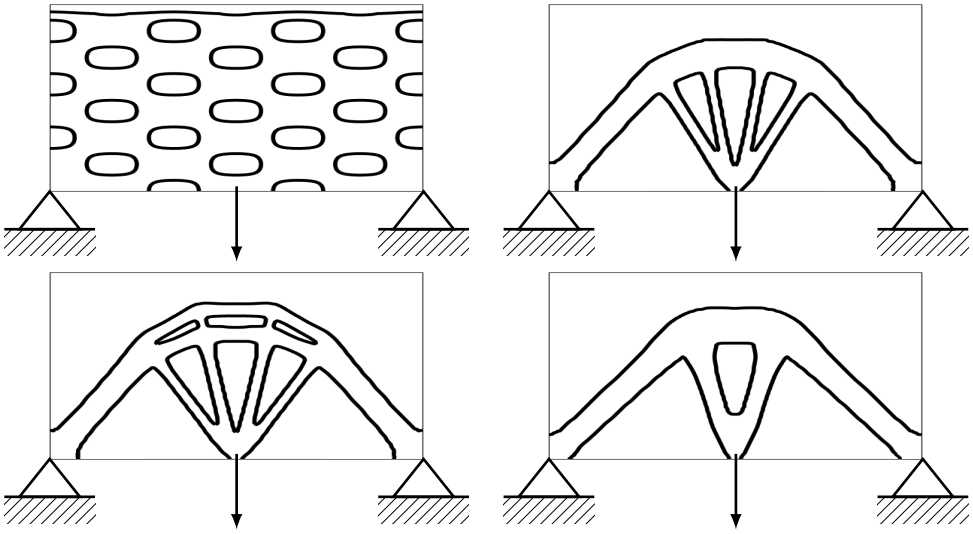

FIG. 5.5. *Bridge problem under material uncertainty: initial design (top left), optimal designs* $\Omega_{\text{det,opt}}$ *(top right),* $\Omega_{\beta=0,\text{opt}}$ *(bottom left) and* $\Omega_{\beta=1,\text{opt}}$ *(bottom right).*

into $\partial\Omega_{N,g}$, over which $g \neq 0$ and is fixed (i.e., non-designable) and $\partial\Omega_{N,0}$, over which $g = 0$ and is optimized.

Starting with the same initial shape, we generate two types of optimal designs: $\Omega_{\text{det,opt}}$, which optimizes the nominal compliance (i.e., for $\xi = 0$); and $\Omega_{\text{stoch,opt}}$, which optimizes a weighted sum of the mean and standard deviation (2.8). For each optimal design, we compute the nominal compliance $J_{\text{nom}}$ (corresponding to $\xi = 0$), the mean $\mu_J$, and a weighted sum of the mean and the standard deviation $\mu_J + \beta\sigma_J$ for $\beta > 0$. The mean $\mu_J$ and standard deviation $\sigma_J$ are estimated using a Monte Carlo estimate with a sample size of 20,000.

**5.2.1. One-dimensional material uncertainty.** We first consider a bridge problem shown in Fig. 5.5. The working domain is $\mathcal{D} = [0, 2] \times [0, 1]$, the volume fraction is $V_{\text{req}}/|\mathcal{D}| = 0.25$, and the deterministic load $g = (0, -1)^T$ is applied to the middle of the bottom boundary. The spatially varying random Young's modulus is given by $E(x, \xi) = E_0(1 + 0.95x_2\xi)$, where $E_0 = 1$ is the nominal Young's modulus, and $\xi \sim \mathcal{U}[-1, 1]$. We consider three objective functions: (i) the nominal compliance $J_{\text{nom}}$ (ii) the mean compliance $\mu_J$ (i.e. (2.8) with $\beta = 0$), and (iii) the sum of the mean and standard deviation of the compliance $\mu_J + \sigma_J$ (i.e., (2.8) with $\beta = 1$).

Fig. 5.5 shows the three optimized designs associated with the three objective functions. The three compliance objective functions, $J_{\text{nom}}$, $\mu_J$, and $\mu_J + \sigma_J$, for each optimized design are shown in Table 5.1. As expected, each optimized design performs best for the associated optimized metric. The design optimized for $\mu_J + \sigma_J$ also yields the best worst-case compliance.

**5.2.2. Random-field material uncertainty: moderate-dimensional case.** We consider a half-wheel problem over a working domain $\mathcal{D} = [0, 2] \times [0, 1.5]$ with a point load at the midpoint of the bottom boundary and a random materials model studied in [35]. The volume fraction $V_{\text{req}}/|\mathcal{D}|$ is set to 0.3. The random Young's modulus field is given by $E(x, \xi) = \exp(c_0(x)+c_1(x)U(x, \xi))$, where $c_0(x) = \log\left(\frac{1}{(1+\text{Var}(x))^{1/2}}\right)$,

| | $J_{\text{nom}}$ | $\mu_J$ | $\mu_J + \sigma_J$ | $\max_\xi J(\xi)$ |
|---|---|---|---|---|
| $J_{\text{nom}}$-optimized design | **15.41** | 16.49 | 19.98 | 26.01 |
| $\mu_J$-optimized design | 15.49 | **16.38** | 19.89 | 25.49 |
| $\mu_J + \sigma_J$-optimized design | 15.90 | 16.70 | **19.74** | **24.51** |

TABLE 5.1

*Comparison of nominal ($J_{\text{nom}}$), robust ($\mu_J$ and $\mu_J + \sigma_J$), and worst ($\max_\xi J(\xi)$) case compliance values for bridge problem under material uncertainties.*

| | $J_{\text{nom}}$ | $\mu_J$ | $\sigma_J$ |
|---|---|---|---|
| $J_{\text{nom}}$-optimized design | **14.45** | 14.86 | 2.60 |
| $\mu_J$-optimized design | 14.47 | **14.69** | 2.57 |
| $\mu_J + 2\sigma_J$-optimized design | 14.52 | 14.71 | 2.54 |
| $\mu_J + 10\sigma_J$-optimized design | 14.80 | 15.08 | **2.50** |

TABLE 5.2

*Comparison of nominal, mean, and standard deviation of compliance for various optimized designs for the half-wheel problem under moderate-dimensional material uncertainties with $M = 8$ random variables.*

$c_1(x) = (\log(1 + \text{Var}(x)))^{1/2}$, $\text{Var}(x) = \left(3.456x^2 - 0.6856x\right)^2$. The zero-mean Gaussian random field $U(x, \xi)$ associated with the covariance kernel $C(x, y) = e^{-\frac{||x-y||^2}{l^2}}$ with the correlation length $l = 8$ is approximated using a KL expansion truncated with $M = 8$ terms, which captures 99% of the energy. Note that $c_0(x)$ and $c_1(x)$ controls the mean and variance of the log-normal random field.

We optimize the design for (i) the nominal compliance $J_{\text{nom}}$ (associated with $\xi = 0$) as well as (ii) the robustness metric $\mu_J + \beta\sigma_J$ for $\beta \in \{0, 2, 10\}$ using the first-order AAPG method. Fig. 5.6 shows the optimized structures. We observe that the number of load paths increases with the standard deviation weighting $\beta$. This provides structural redundancy, leading to less variation in the compliance when subject to material uncertainty, at the cost of nominal (and mean) compliance. Table 5.2 provides a quantitative comparison of the nominal compliance $J_{\text{nom}}$, the mean compliance $\mu_J$, and the standard deviation $\sigma_J$ for the four designs. As expected, $J_{\text{nom}}$- and $\mu_J$-optimized designs perform best in the respective metrics; $\mu_J + 10\sigma_J$-optimized design, with the highest penalty $\beta$ on the standard deviation, yields the smallest $\sigma_J$.

**5.2.3. Random-field material uncertainty: higher-dimensional case.** To demonstrate the ability of the AAPG method to handle problems with a larger number of random variables, we again consider the half-wheel problem with the same form of a random Young's modulus field. However, in this case, we shorten the correlation length to $l = 6$ and choose $M = 31$-term KL expansion to capture 99.99% of the energy. We optimize the design for (i) the nominal compliance $J_{\text{nom}}$ (associated with $\xi = 0$) as well as (ii) the robustness metric $\mu_J + \beta\sigma_J$ for $\beta = 1$ using the first-order AAPG method. Fig. 5.7 shows the robust-optimized structure, with a nominal compliance of 14.51 and a robust compliance, with $\beta = 1$, of 17.08. The nominal-optimized design $\Omega_{\text{det,opt}}$ yields a nominal compliance of 14.45 and a robustness metric, with $\beta = 1$, of 17.24. (The nominal optimized design $\Omega_{\text{det,opt}}$ is the same as that reported in Section 5.2.2; however, the associated robustness metric is different because the random material is different.) We recall that the computational cost of the first-order AAPG method scales linearly with $M$ (compared to other methods that scale less favorably), which enables the solution of this higher-dimensional problem. For our

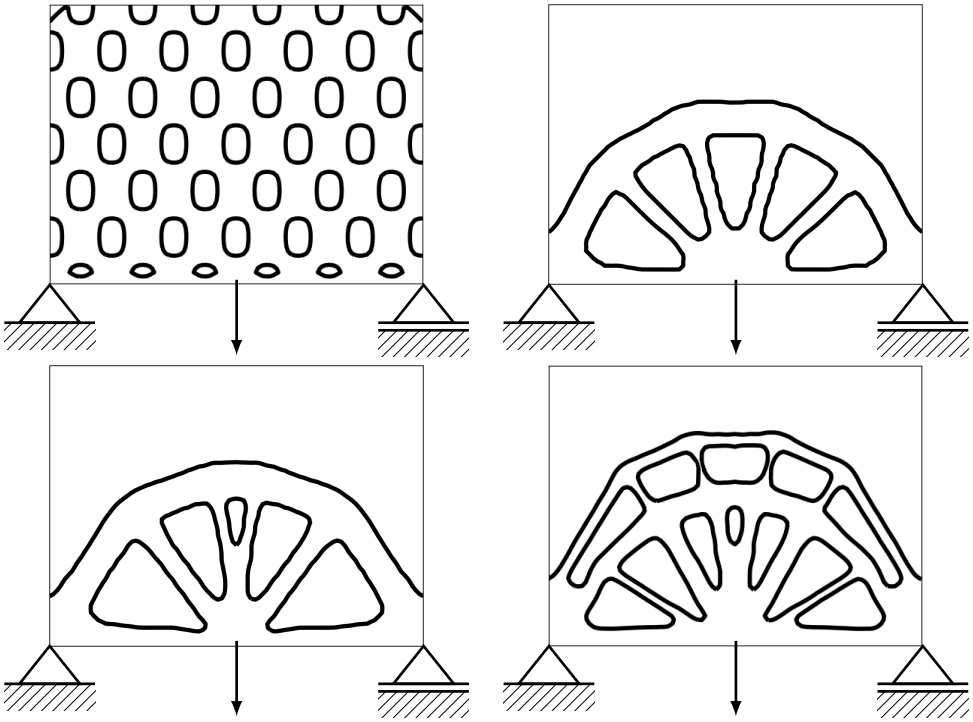

FIG. 5.6. *Half-wheel problem under moderate-dimensional material uncertainties with $M = 8$ random variables: initial design (top left), optimal designs $\Omega_{det,opt}$ (top right), $\Omega_{\beta=0,opt}$ (bottom left) and $\Omega_{\beta=10,opt}$ (bottom right).*

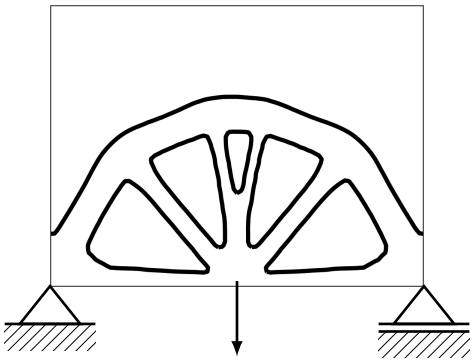

FIG. 5.7. *Half-wheel problem under higher-dimensional material uncertainties with $M = 31$ random variables: robust-optimal design $\Omega_{\beta=1,\mathrm{opt}}$.*

current (sequential) implementation, the computational time for this $M = 31$ case is $\approx 2.3$ times the computational time for the $M = 8$ case; the favorable sublinear scaling is due to a fewer number of quadrature points required for higher modes with smaller influences.

**5.2.4. Assessment of the computational costs.** In order to assess the computational cost and accuracy of the AAPG method, we revisit the half-wheel problem under material uncertainty with $M = 8$ considered in Section 5.2.2. We solve the prob-

| | $\mu_J$ | $\sigma_J$ | approximate cost (solves) |
|---|---|---|---|
| **quasi-Monte Carlo** | **14.88275** | **2.58944** | 8192 |
| first-order AAPG $\ell = 8$ | 14.88136 | 2.55287 | 42 |
| first-order AAPG $\ell = 5$ | 14.87332 | 2.52687 | 28 |
| first-order AAPG $\ell = 2$ | 14.83000 | 2.37719 | 17 |
| sparse PC $\ell = 2$ | 14.87778 | 2.55282 | 161 |
| sparse PC $\ell = 1$ | 14.81387 | 2.26970 | 17 |

TABLE 5.3

*The mean ($\mu_J$) and standard deviation ($\sigma_J$) computed using the "reference" quasi-Monte Carlo method, first-order AAPG, and PC.*

lem using three methods: (i) a quasi-Monte Carlo method; (ii) a first-order AAPG method; and (iii) PC with anisotropic sparse grid.

Our anisotropic sampling approach follows the method used in [35] based on an adaptive anisotropic sparse grid collocation method from [39]. Namely, as the material uncertainty is defined by a KL expansion, we *assume* the random variables associated with the terms involving the larger eigenvalues are more important and adjust the polynomial degrees accordingly. Specifically, we construct the anisotropic Smolyak sparse grid as follows. Given a sparse grid level $\ell \in \mathbb{N}_+$, we first introduce the index set $\mathbf{X}_\zeta(\ell, N) = \left\{\mathbf{i} = (i_1, \ldots, i_N) \in \mathbb{N}_+^N, \mathbf{i} \geq \mathbf{1} : \sum_{n=1}^N (i_n - 1)\,\zeta_n \leq \ell\underline{\zeta}\right\}$, where $\zeta = (\zeta_1, \zeta_2, \ldots, \zeta_N)$ is a set of weights for the different stochastic dimensions, and $\underline{\zeta} := \min_{1\leq n\leq N} \zeta_n$. Here, given a KL expansion with Gaussian random variables, we choose $\zeta_n = \frac{1}{2\sqrt{2}\sqrt{\lambda_n}\|\phi_n\|_{L^\infty(D)}}$, where $\{\lambda_n, \phi_n(x)\}$ is the eigenpair in the KL expansion. We then set the PC degree associated with the $j$-th random variable to $p_{\xi_j} = (i_j - 1)\zeta_j \leq \ell\underline{\zeta}$. For consistency, we also use this approach to determine an appropriate PC degree for each subproblem of the first-order AAPG approximation.

We compare the cost and accuracy of the first-order AAPG and the PC method on a fixed design. Table 5.3 shows the mean and standard derivation computed using (a) quasi-Monte Carlo with a sample size of 8192, which serves as the reference solution; (b) first-order AAPG with the sparse grid levels $\ell \in \{2, 5, 8\}$; and (c) the PC method with the sparse grid levels $\ell \in \{1, 2\}$. The cost estimate for the AAPG and sparse PC methods are based on the assumption that the cost to solve a PC system scales linearly with the number of terms in the PC expansion; e.g., the cost to solve a PC system with $N_\xi$ terms is $N_\xi$ times the cost of a single deterministic solve. The results show that, for the materials UQ problem with $M = 8$ random variables, the $\ell = 2$ AAPG provides more accurate mean and standard deviation than the $\ell = 1$ PC at the same cost. Similarly, the $\ell = 8$ AAPG provides more accurate mean and standard derivation than the $\ell = 2$ PC at $\sim 1/4$ of the cost. Specifically, the $\ell = 8$ AAPG method achieves the relative mean error of $\sim 10^{-5}$ and the relative standard deviation error of $\sim 10^{-2}$. The efficiency of the first-order AAPG method allows us to perform robust TO on a single commodity desktop computer for this problem.

**5.2.5. Sensitivity to the choice of anchor point.** We finally assess the sensitivity of the AAPG approximation to the choice of the anchor point $\xi^a$. In general, finding the optimal anchor point is impractical due to high computational cost [4]. We hence compare two different choices of anchor points, which are practically computable and we hope are effective: the anchor point $\xi^{a0}$ at the centroid of $\Gamma$, which has been used throughout this work; an alternate anchor point $\xi^{a*}$ that yields the

solution close to the mean in the sense that

$$\xi^{a*} = \underset{i\in\{1,\dots,M\}}{\arg\min}\ \mathcal{A}(u(\cdot,\xi^{(i)}) - \langle u\rangle_\Gamma, u(\cdot,\xi^{(i)}) - \langle u\rangle_\Gamma), \tag{5.2}$$

where $\{\xi^{(i)}\}_{i=1}^M \subset \Gamma$ is a set of $M$ candidate points (chosen randomly) [34, 41, 45, 49].

For the same fixed design used in Section 5.2.4, we compute the mean and variance of the compliance for the $L = 1$, $\ell = 8$ AAPG approximations associated with anchor points $\xi^{a0}$ and $\xi^{a*}$ found for $M = 1000$. As shown in Table 5.3, the reference quasi-Monte Carlo method yields the mean and variance of 14.88275 and 2.58944, respectively. For the anchor point $\xi^{a0}$, the mean and variance are 14.88136 and 2.55287, respectively. For the alternative anchor point $\xi^{a*}$, the mean and variance are 14.88171 and 2.56115, respectively. The alternative anchor point $\xi^{a*}$ yields a slightly more accurate mean and variance than $\xi^{a0}$; however the difference is arguably negligible. In addition, in topology optimization, we would have to solve (5.2) to find $\xi^{a*}$ for each new geometry, which would render the approach computationally uncompetitive. Hence, we have used the centroid anchor point $\xi^{a0}$ throughout this work.

**6. Conclusion.** In this paper, we presented an approach for robust structural topology optimization, for mean- and variance-based robustness metrics of a linear functional output in the presence of uncertainties in the loading and material properties. We employed the AAPG projection scheme for the governing linear elasticity SPDEs to provide an efficient approximation of higher-dimensional problems. We then developed formulations to efficiently evaluate the robustness metric and the associated shape derivative that are non-intrusive and semi-intrusive for loading and materials uncertainty, respectively. We finally assessed the accuracy and computational efficiency of the proposed AAPG-based approach using a series of numerical examples. Comparisons with gPC approaches show that the AAPG approach can provide accuracy similar to gPC methods at significantly lower computational costs.

**Acknowledgments.** The financial support for this work was provided by Autodesk Research and the Natural Sciences and Engineering Research Council of Canada.

**Appendix A. Parametrization of material properties.** Consider isotropic materials whose elasticity properties are described by the Hooke's law $AX = 2\mu X + \lambda \mathrm{Tr}(X)I$, for any $X \in \mathbb{R}^{d\times d}$. The Lamé coefficients satisfy the conditions $\mu > 0$ and $\lambda + 2\mu/d > 0$ and can be written as $\mu = \frac{E}{2(1+\nu)}$ and $\lambda = \frac{E\nu}{(1+\nu)(1-2\nu)}$, where $E$ is the Young's modulus and $\nu$ is the Poisson ratio. We assume that the Young's modulus is discretized using a KL expansion [32] $E(x,\xi) = \overline{E}(x) + \sum_{i=1}^M \xi_i E_i(x)$, where $(\xi_i)_i$ are independent and identically distributed random variables. The spatial modes are defined as $E_i(x) = \sigma_E\sqrt{\lambda_i}\phi_i(x)$, where $\phi_i$ is the solution of the eigenproblem $\int_\Omega C_E(x,y)\phi_i(y)dy = \lambda_i\phi_i(x)$, $||\phi_i||_{L^2(\Omega)} = 1$ where $C_E$ denotes the two-point correlation function used for modeling the Young's modulus. By linearity of Lamé coefficients in $E$, the KL expansion translates to the Hooke's law as $A(x,\xi)X := 2\overline{\mu}(x)X + \overline{\lambda}(x)\mathrm{Tr}(X) + \sum_{i=1}^M \xi_i\Big(2\mu_i(x)X + \lambda_i(x)\mathrm{Tr}(X)I\Big)$ with $\overline{\lambda}(x) = \frac{\nu\overline{E}(x)}{(1+\nu)(1-2\nu)}$, $\overline{\mu}(x) = \frac{\overline{E}(x)}{2(1+\nu)}$, $\lambda_i(x) = \frac{\nu E_i(x)}{(1+\nu)(1-2\nu)}$ and $\mu_i(x) = \frac{E_i(x)}{2(1+\nu)}$.

**Appendix B. Shape derivative of the variance for compliant problems.** We first consider the case of uncertainties arising from both material properties and loading conditions; i.e., $1 \le M_L \le M-1$.

PROPOSITION B.1. *Under Assumptions 2, 3 and 5, the variance of the compliance associated with the first-order AAPG approximation of the random elasticity problem (2.2) is given by*

$$\begin{aligned}
\sigma_J^2(u,\Omega) \simeq & \sum_{j_1=1}^{M} \big( \langle J(\widetilde{u}^{j_1},\Omega,\cdot)^2 \rangle_{\Gamma_{j_1}} - \langle J(\widetilde{u}^{j_1},\Omega,\cdot) \rangle_{\Gamma_{j_1}}^2 \big) + (1-M)^2 \sum_{i=1}^{M_L} \langle \xi_i^2 \rangle_{\Gamma_i} \mathcal{L}^i(u^0,\Omega)^2 \\
& + 2(1-M) \sum_{j_1=1}^{M} \left( \sum_{i \neq j_1}^{M_L} \langle \xi_i^2 \rangle_{\Gamma_i} \mathcal{L}^i(u^0,\Omega) \langle \mathcal{L}^i(\widetilde{u}^{j_1},\Omega) \rangle_{\Gamma_{j_1}} + \langle \xi_{j_1} J(\widetilde{u}^{j_1},\Omega,\cdot) \rangle_{\Gamma_{j_1}} \mathcal{L}^{j_1}(u^0,\Omega) \right) \\
& + 2 \sum_{j_1 \neq k_1}^{M} \langle \xi_{j_1} J(\widetilde{u}^{j_1},\Omega,\cdot) \rangle_{\Gamma_{j_1}} \langle \mathcal{L}^{j_1}(\widetilde{u}^{k_1},\Omega) \rangle_{\Gamma_{k_1}} \\
& + \sum_{j_1=1}^{M} \sum_{k_1=1}^{M} \big( D_{j_1}(\widetilde{u}^{j_1},\Omega) \delta_{j_1,k_1} + E_{j_1,k_1}(\widetilde{u}^{j_1},\widetilde{u}^{k_1},\Omega)(1-\delta_{j_1,k_1}) \big),
\end{aligned} \tag{B.1}$$

*where* $D_{j_1}(\widetilde{u}^{j_1},\Omega) = \sum_{i \neq j_1}^{M_L} \langle \xi_i^2 \rangle_{\Gamma_i} \langle \mathcal{L}^i(\widetilde{u}^{j_1},\Omega)^2 \rangle_{\Gamma_{j_1}}$, *and*

$$\begin{aligned}
E_{j_1,k_1}(\widetilde{u}^{j_1},\widetilde{u}^{k_1},\Omega) = & \sum_{i \neq (j_1,k_1)}^{M_L} \langle \xi_i^2 \rangle_{\Gamma_i} \langle \mathcal{L}^i(\widetilde{u}^{j_1},\Omega) \rangle_{\Gamma_{j_1}} \langle \mathcal{L}^i(\widetilde{u}^{k_1},\Omega) \rangle_{\Gamma_{k_1}} \\
& + \langle \xi_{j_1} \mathcal{L}^{k_1}(\widetilde{u}^{j_1},\Omega) \rangle_{\Gamma_{j_1}} \langle \xi_{k_1} \mathcal{L}^{j_1}(\widetilde{u}^{k_1},\Omega) \rangle_{\Gamma_{k_1}}.
\end{aligned}$$

*Proof.* Under Assumption 5, $\overline{\mathcal{L}}_o(u^0,\Omega) = J(u^0,\Omega)$ and $\overline{\mathcal{L}}(\widetilde{u}^{j_1},\Omega) + \xi_{j_1}\mathcal{L}^{j_1}(\widetilde{u}^{j_1},\Omega) = J(\widetilde{u}^{j_1},\Omega,\xi_{j_1})$. Then it follows

$$\begin{aligned}
J(\widehat{u}^1,\Omega,\xi) = & (1-M)J(u^0,\Omega) + \sum_{j_1=1}^{M} J(\widetilde{u}^{j_1},\Omega,\xi_{j_1}) \\
& + (1-M) \sum_{i=1}^{M_L} \xi_i \mathcal{L}^i(u^0,\Omega) + \sum_{j_1=1}^{M} \sum_{i \neq j_1}^{M_L} \xi_i \mathcal{L}^i(\widetilde{u}^{j_1},\Omega)
\end{aligned} \tag{B.2}$$

and $\mu_J(\widehat{u}^1,\Omega) = (1-M)J(u^0,\Omega) + \sum_{j_1=1}^{M} \langle J(\widetilde{u}^{j_1},\Omega,\cdot) \rangle_{\Gamma_{j_1}}$ from which we deduce (B.1) after reorganizing terms in $\sigma_J^2(u,\Omega) = \langle J(\widehat{u}^1,\Omega,\cdot)^2 \rangle_\Gamma - \mu_J(\widehat{u}^1,\Omega)^2$. ∎

Hence, estimating the shape derivative $D_\Omega\big(\sigma_J^2(\widehat{u}^1,\Omega)\big)$ requires computing the terms $(D_\Omega\big(J(\widetilde{u}^{j_1},\Omega,\xi_{j_1}^{(i)})\big))_{j_1=1,\dots,M}$ and the shape derivatives of the output functions $(D_\Omega\big(\mathcal{L}^{j_1}(u^0,\Omega)\big))_{j_1=1,\dots,M_L}$ and $(D_\Omega\big(\mathcal{L}^{j_1}(\widetilde{u}^{k_1}(\cdot,\xi_{k_1}^{(i)}),\Omega)\big))_{k_1=1,\dots,M,j_1\neq k_1}$ at the quadrature points $(\xi_{k_1}^{(i)})_{i=1,\dots,N_Q}$, which requires the solution of $M_L + (M-1)M_L N_Q$ deterministic adjoint problems.

We next examine cases where the randomness arises exclusively from uncertainties on the material properties or from the loading conditions. In such cases, we obtain simpler and fully non-intrusive expressions for the shape sensitivities of $\sigma_J^2$, without adjoint solutions. As a reminder, the shape derivative of the mean compliance is fully non-intrusive even in the case of mixed uncertainties (see Proposition 4.2).

**B.1. Uncertainties in the material properties.** We assume the loading terms $f$ and $g$ are both deterministic; i.e., the randomness arise exclusively from material uncertainties ($M_L = 0$). Using a first-order AAPG approximation, the random compliance can be expanded as $J(u,\Omega,\xi) \simeq (1-M)J(u^0,\Omega) +$

$\sum_{j_1=1}^{M} J(\widetilde{u}^{j_1},\Omega,\xi_{j_1})$ which is a simplified version of (B.2). Consequently, it holds $\sigma_J^2(u,\Omega) \simeq \sum_{j_1=1}^{M}\big(\langle J(\widetilde{u}^{j_1},\Omega,\cdot)^2\rangle_{j_1} - \langle J(\widetilde{u}^{j_1},\Omega,\cdot)\rangle_{j_1}^2\big)$ and

$$\begin{aligned} D_\Omega\big(\sigma_J^2(u,\Omega)\big) \quad &\simeq 2\sum_{j_1=1}^{M}\Big(\langle J(\widetilde{u}^{j_1},\Omega,\cdot) D_\Omega\big(J(\widetilde{u}^{j_1},\Omega,\cdot)\big)\rangle_{j_1} \\ &\quad -\langle J(\widetilde{u}^{j_1},\Omega,\cdot)\rangle_{j_1}\langle D_\Omega\big(J(\widetilde{u}^{j_1},\Omega,\cdot)\big)\rangle_{j_1}\Big), \end{aligned} \tag{B.3}$$

which can be approximated using one-dimensional quadrature rules.

**B.2. Uncertainties in the loading conditions.** The randomness originates here from uncertainties on the loading conditions only ($M_L = M$). By linearity of the operator in (2.2) and using Assumption 3, the random elasticity solution is given by $u(x,\xi) = u^0(x) + \sum_{i=1}^{M}\xi_i u^i(x)$, where $u^0$ (resp. $u^i$) is the solution of a deterministic elasticity problem with loading terms $\overline{\phi}$ and $\overline{\psi}$ (resp. $\phi_i$ and $\psi_i$). In this setting, exact and fully non-intrusive expressions for the shape derivatives of the statistical moments of $J$ are given by $D_\Omega\big(\mu_J(u,\Omega)\big) = D_\Omega\big(J(u^0,\Omega)\big) + \sum_{i=1}^{M}\langle\xi_i^2\rangle_{\Gamma_i} D_\Omega\big(J(u^i,\Omega)\big)$ and

$$\begin{aligned} D_\Omega\big(\sigma_J^2(u,\Omega)\big) &= 2\sum_{i=1}^{M}\langle\xi_i^2\rangle_{\Gamma_i}\big(J(u^i,\Omega) + J(u^0,\Omega) - J(u^0-u^i,\Omega)\big) \\ &\qquad \times D_\Omega\big(J(u^i,\Omega) + J(u^0,\Omega) - J(u^0-u^i,\Omega)\big) \\ &\quad + 2\sum_{i=1}^{M}\langle\xi_i^4\rangle_{\Gamma_i} J(u^i,\Omega) D_\Omega\big(J(u^i,\Omega)\big) - 2\sum_{i,j=1}^{M}\langle\xi_i^2\rangle_{\Gamma_i}\langle\xi_j^2\rangle_{\Gamma_j} J(u^i,\Omega) D_\Omega\big(J(u^j,\Omega)\big), \end{aligned} \tag{B.4}$$

using the fact that the random variables are centered.

## REFERENCES


[1] David Adalsteinsson and James A Sethian, *The fast construction of extension velocities in level set methods*, Journal of Computational Physics, 148 (1999), pp. 2–22.

[2] Grégoire Allaire and Charles Dapogny, *A deterministic approximation method in shape optimization under random uncertainties*, The SMAI journal of computational mathematics, 1 (2015), pp. 83–143.

[3] Grégoire Allaire, François Jouve, and Anca-Maria Toader, *Structural optimization using sensitivity analysis and a level-set method*, Journal of computational physics, 194 (2004), pp. 363–393.

[4] Christophe Audouze and Prasanth B. Nair, *Anchored anova petrov-galerkin projection schemes for parabolic stochastic partial differential equations*, Computational Methods in Applied Mechanics and Engineering, 276 (2014), pp. 362–395.

[5] Kyoung-ryun Bae and Semyung Wang, *Reliability-based topology optimization*, in 9th AIAA/ISSMO symposium on multidisciplinary analysis and optimization, 2002, p. 5542.

[6] Susanne C Brenner and L Ridgway Scott, *The mathematical theory of finite element methods*, vol. 3, Springer, 2008.

[7] Jean Céa, *Conception optimale ou identification de formes, calcul rapide de la dérivée directionnelle de la fonction coût*, ESAIM: Mathematical Modelling and Numerical Analysis-Modélisation Mathématique et Analyse Numérique, 20 (1986), pp. 371–402.

[8] Shikui Chen and Wei Chen, *A new level-set based approach to shape and topology optimization under geometric uncertainty*, Structural and Multidisciplinary Optimization, 44 (2011), pp. 1–18.

[9] Shikui Chen, Wei Chen, and Sanghoon Lee, *Level set based robust shape and topology optimization under random field uncertainties*, Structural and Multidisciplinary Optimization, 41 (2010), pp. 507–524.

[10] Sergio Conti, Harald Held, Martin Pach, Martin Rumpf, and Rüdiger Schultz, *Shape optimization under uncertainty—a stochastic programming perspective*, SIAM Journal on Optimization, 19 (2009), pp. 1610–1632.
[11] Subhayan De, Jerrad Hampton, Kurt Maute, and Alireza Doostan, *Topology optimization under uncertainty using a stochastic gradient-based approach*, Structural and Multidisciplinary Optimization, 62 (2020), pp. 2255–2278.
[12] Frédéric De Gournay, *Velocity extension for the level-set method and multiple eigenvalues in shape optimization*, SIAM journal on control and optimization, 45 (2006), pp. 343–367.
[13] Joshua D Deaton and Ramana V Grandhi, *A survey of structural and multidisciplinary continuum topology optimization: post 2000*, Structural and Multidisciplinary Optimization, 49 (2014), pp. 1–38.
[14] Peter D Dunning, H Alicia Kim, and Glen Mullineux, *Introducing loading uncertainty in topology optimization*, AIAA journal, 49 (2011), pp. 760–768.
[15] Young-Sop Eom, Kwang-Sun Yoo, Jae-Yong Park, and Seog-Young Han, *Reliability-based topology optimization using a standard response surface method for three-dimensional structures*, Structural and multidisciplinary optimization, 43 (2011), pp. 287–295.
[16] Zhen Gao and Jan S Hesthaven, *On anova expansions and strategies for choosing the anchor point*, Applied Mathematics and Computation, 217 (2010), pp. 3274–3285.
[17] Roger G Ghanem and Pol D Spanos, *Stochastic finite elements: a spectral approach*, Courier Corporation, 2003.
[18] Michael Griebel, *Sparse grids and related approximation schemes for higher dimensional problems*, Citeseer, 2005.
[19] James K Guest and Takeru Igusa, *Structural optimization under uncertain loads and nodal locations*, Computer Methods in Applied Mechanics and Engineering, 198 (2008), pp. 116–124.
[20] Miche Jansen, Geert Lombaert, and Mattias Schevenels, *Robust topology optimization of structures with imperfect geometry based on geometric nonlinear analysis*, Computer Methods in Applied Mechanics and Engineering, 285 (2015), pp. 452–467.
[21] Hyun-Seung Jung and Seonho Cho, *Reliability-based topology optimization of geometrically nonlinear structures with loading and material uncertainties*, Finite elements in analysis and design, 41 (2004), pp. 311–331.
[22] Vahid Keshavarzzadeh, Felipe Fernandez, and Daniel A Tortorelli, *Topology optimization under uncertainty via non-intrusive polynomial chaos expansion*, Computer Methods in Applied Mechanics and Engineering, 318 (2017), pp. 120–147.
[23] Ghais Kharmanda, Niels Olhoff, A Mohamed, and Maurice Lemaire, *Reliability-based topology optimization*, Structural and Multidisciplinary optimization, 26 (2004), pp. 295–307.
[24] Chwail Kim, Semyung Wang, Kyoung-ryun Rae, Heegon Moon, and Kyung K Choi, *Reliability-based topology optimization with uncertainties*, Journal of mechanical science and technology, 20 (2006), pp. 494–504.
[25] Aaron Klein, Prasanth B Nair, and Masayuki Yano, *A priori error analysis of shape derivatives of linear functionals in structural topology optimization*, Computer Methods in Applied Mechanics and Engineering, 395 (2022), p. 114991.
[26] Omar M Knio, Habib N Najm, Roger G Ghanem, et al., *A stochastic projection method for fluid flow: I. basic formulation*, Journal of computational Physics, 173 (2001), pp. 481–511.
[27] Benedikt Kriegesmann, *Robust design optimization with design-dependent random input variables*, Structural and multidisciplinary optimization, 61 (2020), pp. 661–674.
[28] Antoine Laurain, *A level set-based structural optimization code using fenics*, Structural and Multidisciplinary Optimization, 58 (2018), pp. 1311–1334.
[29] Antoine Laurain and Kevin Sturm, *Distributed shape derivative via averaged adjoint method and applications*, ESAIM: Mathematical Modelling and Numerical Analysis, 50 (2016), pp. 1241–1267.
[30] Boyan S Lazarov, Mattias Schevenels, and Ole Sigmund, *Topology optimization considering material and geometric uncertainties using stochastic collocation methods*, Structural and Multidisciplinary optimization, 46 (2012), pp. 597–612.
[31] Olivier P Le Maitre, Matthew T Reagan, Habib N Najm, Roger G Ghanem, and Omar M Knio, *A stochastic projection method for fluid flow: Ii. random process*, Journal of computational Physics, 181 (2002), pp. 9–44.
[32] M. Loève, *Probability theory*, in fourth ed, Springer, 1977.
[33] Didier Lucor and George Em Karniadakis, *Noisy inflows cause a shedding-mode switching in flow past an oscillating cylinder*, Physical review letters, 92 (2004), p. 154501.

[34] Xiang Ma and Nicholas Zabaras, *An adaptive high-dimensional stochastic model representation technique for the solution of stochastic partial differential equations*, Journal of Computational Physics, 229 (2010), pp. 3884–3915.

[35] Jesus Martinez-Frutos, David Herrero-Perez, Mathieu Kessler, and Francisco Periago, *Robust shape optimization of continuous structures via the level set method*, Computer Methods in Applied Mechanics and Engineering, 305 (2016), pp. 271–291.

[36] Hermann G Matthies and Andreas Keese, *Galerkin methods for linear and nonlinear elliptic stochastic partial differential equations*, Computer methods in applied mechanics and engineering, 194 (2005), pp. 1295–1331.

[37] Katsuya Mogami, Shinji Nishiwaki, Kazuhiro Izui, Masataka Yoshimura, and Nozomu Kogiso, *Reliability-based structural optimization of frame structures for multiple failure criteria using topology optimization techniques*, Structural and Multidisciplinary Optimization, 32 (2006), pp. 299–311.

[38] Prasanth B Nair, Pär Hakansson, and Christophe Audouze, *Prospects for overcoming the curse of dimensionality in polynomial chaos based stochastic projection schemes*, in Proc. of the 4th European Conf. on Computational Mechanics. Paris, France. See https://www. eccm-2010. org/abstract_ pdf/abstract_1952. pdf, 2010.

[39] Fabio Nobile, Raul Tempone, and Clayton G Webster, *An anisotropic sparse grid stochastic collocation method for partial differential equations with random input data*, SIAM Journal on Numerical Analysis, 46 (2008), pp. 2411–2442.

[40] Herschel Rabitz and Ömer F Aliş, *General foundations of high-dimensional model representations*, Journal of Mathematical Chemistry, 25 (1999), pp. 197–233.

[41] Herschel Rabitz, Ömer F Aliş, Jeffrey Shorter, and Kyurhee Shim, *Efficient input—output model representations*, Computer physics communications, 117 (1999), pp. 11–20.

[42] Ole Sigmund and Kurt Maute, *Topology optimization approaches: A comparative review*, Structural and Multidisciplinary Optimization, 48 (2013), pp. 1031–1055.

[43] Jacques Simon, *Differentiation with respect to the domain in boundary value problems*, Numerical Functional Analysis and Optimization, 2 (1980), pp. 649–687.

[44] Ralph C Smith, *Uncertainty quantification: theory, implementation, and applications*, vol. 12, Siam, 2013.

[45] IM Sobol, *Theorems and examples on high dimensional model representation*, Reliability Engineering and System Safety, 79 (2003), pp. 187–193.

[46] Jan Sokolowski and JP Zolesio, *Introduction to shape optimization: Shape sensitivity analysis*, 1992.

[47] Mazdak Tootkaboni, Alireza Asadpoure, and James K Guest, *Topology optimization of continuum structures under uncertainty–a polynomial chaos approach*, Computer Methods in Applied Mechanics and Engineering, 201 (2012), pp. 263–275.

[48] Shengyin Wang and Michael Yu Wang, *Radial basis functions and level set method for structural topology optimization*, International journal for numerical methods in engineering, 65 (2006), pp. 2060–2090.

[49] Xiaoqun Wang, *On the approximation error in high dimensional model representation*, in 2008 Winter Simulation Conference, IEEE, 2008, pp. 453–462.

[50] Dongbin Xiu and Jan S Hesthaven, *High-order collocation methods for differential equations with random inputs*, SIAM Journal on Scientific Computing, 27 (2005), pp. 1118–1139.

[51] Dongbin Xiu and George Em Karniadakis, *Modeling uncertainty in steady state diffusion problems via generalized polynomial chaos*, Computer methods in applied mechanics and engineering, 191 (2002), pp. 4927–4948.

[52] Hequin Xu and Sharif Rahman, *A generalized dimension-reduction method for multidimensional integration in stochastic mechanics*, International Journal for Numerical Methods in Engineering, 61 (2004), pp. 1992–2019.

[53] Xiu Yang, Minseok Choi, Guang Lin, and George Em Karniadakis, *Adaptive anova decomposition of stochastic incompressible and compressible flows*, Journal of Computational Physics, 231 (2012), pp. 1587–1614.

[54] T.A. Zang, M.J. Hemsch, M.W. Hilburger, S.P. Kenny, J.M. Luckring, P. Maghami, S.L. Padula, and W.J. Stroud, *Needs and opportunities for uncertainty-based multidisciplinary design methods for aerospace vehicles*, National Aeronautics and Space Administration, Langley Research Center, 2002.

[55] Zhongqiang Zhang, Minseok Choi, and George Em Karniadakis, *Anchor points matter in anova decomposition*, in Spectral and High Order Methods for Partial Differential Equations, Springer, 2011, pp. 347–355.

[56] Junpeng Zhao and Chunjie Wang, *Robust topology optimization of structures under loading uncertainty*, AIAA journal, 52 (2014), pp. 398–407.